

[8] Dipolar Couplings in Macromolecular Structure Determination

By AD BAX, GEORG KONTAXIS, and NICO TJANDRA

1. Introduction

Structure determination by nuclear magnetic resonance (NMR) traditionally has relied on the measurement of a maximum possible number of semiquantitative local restraints. The most important of these is the ^1H - ^1H nuclear Overhauser effect (NOE), which provides distance information for pairs of protons separated by less than ca 5 Å. The accuracy of the NOE-derived distance usually decreases with the actual value of the distance because the effect of indirect NOE magnetization transfer (spin diffusion) tends to be worse for protons further apart. The second commonly used restraint is the three-bond J coupling, either homonuclear ^1H - ^1H , ^{13}C - ^{13}C , or heteronuclear ^{13}C - ^1H , ^{13}C - ^{15}N , or ^{15}N - ^1H , which are related to the intervening dihedral angles via empirically parameterized Karplus relationships.¹⁻³ Numerous methods have been proposed in recent years for the measurement of such couplings.⁴⁻⁶ It has been shown possible to measure J -coupling interaction through hydrogen bonds, providing yet another important restraint and permitting the hydrogen bond donor and acceptor atoms to be linked in a completely unambiguous manner.⁷⁻⁹ Another relatively recent addition to the arsenal of experimental restraints includes cross-correlated relaxation.¹⁰⁻¹² In contrast to all other parameters mentioned above, cross-correlated relaxation can, at least in principle, report on the relative orientation of dipolar and chemical

¹ M. Karplus, *J. Phys. Chem.* **30**, 11 (1959).

² V. F. Bystrov, *Prog. NMR Spectr.* **10**, 41 (1976).

³ J. S. Hu and A. Bax, *J. Am. Chem. Soc.* **119**, 6360 (1997).

⁴ A. Bax, G. W. Vuister, S. Grzesiek, F. Delaglio, A. C. Wang, R. Tschudin, and G. Zhu, *Methods Enzymol.* **239**, 79 (1994).

⁵ C. Biamonti, C. B. Rios, B. A. Lyons, and G. T. Montelione, *Adv. Biophys. Chem.* **4**, 51 (1994).

⁶ G. W. Vuister, M. Tessari, Y. Karimi-Nejad, and B. Whitehead, eds., "Pulse Sequences for Measuring Coupling Constants," Vol. 16 of "Biological Magnetic Resonance" (R. Krishna and L. Berliner, eds.), Kluwer, Dordrecht, The Netherlands, 1999.

⁷ A. J. Dingley and S. Grzesiek, *J. Am. Chem. Soc.* **120**, 8293 (1998).

⁸ K. Pervushin, A. Ono, C. Fernandez, T. Szyperski, M. Kainosho, and K. Wüthrich, *Proc. Natl. Acad. Sci. U.S.A.* **95**, 14147 (1998).

⁹ Y. X. Wang, J. Jacob, F. Cordier, P. Wingfield, S. J. Stahl, S. Lee-Huang, D. Torchia, S. Grzesiek, and A. Bax, *J. Biomol. NMR* **14**, 181 (1999).

¹⁰ B. Reif, M. Henning, and C. Griesinger, *Science* **276**, 1230 (1997).

¹¹ D. W. Yang, R. Konrat, and L. E. Kay, *J. Am. Chem. Soc.* **119**, 11938 (1997).

¹² P. Pelupessy, E. Chiarparin, R. Ghose, and G. Bodenhausen, *J. Biomol. NMR* **13**, 375 (1999).

shift anisotropy (CSA) tensors anywhere in the molecule. However, in practice, the requirement to monitor the decay of a two-spin coherence limits this type of information to spatially proximate pairs of spins. Finally, chemical shifts provide yet another source of structural information: There are well characterized relationships between the polypeptide backbone angles ϕ and ψ and $^1\text{H}^\alpha$, $^{13}\text{C}^\alpha$, $^{13}\text{C}^\beta$, and $^{13}\text{C}^\gamma$ chemical shifts, which have been exploited in a variety of ways to improve the quality of protein structures.¹³⁻¹⁷ but again, all contain strictly local information. The main exception has been the paramagnetic shift, which can extend over distances as large as 15–20 Å, and which recently has become the center of renewed interest in structure determination,¹⁸⁻²⁰ precisely because it complements the short-range information contained in the parameters mentioned above.

In recent years, approaches have been developed that reintroduce dipolar couplings into macromolecular solution NMR. Most of today's applications are based on the use of liquid crystalline media, a field with a rich NMR history and first developed by Saupe and Englert.^{21,22} However, the spectral complexity that would be introduced if a macromolecule were subjected to the high degree of order typically obtained in a regular liquid crystal (0.01–0.5) would make the spectrum completely intractable. Therefore, this interesting work largely has been limited to molecules with less than a few dozen nuclei. From a practical perspective, the dipolar studies in macromolecules are closer related to the magnetic alignment work, pioneered by Bothner-By and MacLean.^{23,24} In such studies, the degree of alignment typically is so small that only the strongest dipolar interactions give rise to a residual dipolar coupling, scaled down by a factor of 10^4 to 10^5 relative to its static value. Such a small degree of alignment does not alter the general appearance of the NMR spectrum, but nevertheless permitted the measurement of one-bond ^1H – ^{13}C and geminal ^1H – ^1H couplings,²³ thereby providing information

on the orientation of the corresponding internuclear vectors relative to the magnetic susceptibility tensor.

Tolman *et al.* were the first to apply the magnetic alignment approach to a protein.²⁵ Using paramagnetic myoglobin, uniformly enriched in ^{15}N , they showed a clear field dependence of the one-bond ^1H – ^{15}N splitting that correlated with the orientation of the corresponding internuclear vector relative to the calculated magnetic susceptibility anisotropy tensor. Similar measurements were reported independently and simultaneously by Bolton and co-workers for an unlabeled DNA dodecamer.²⁶ In the latter case, the reported degree of molecular alignment was considerably larger than expected on the basis of calculated values of the susceptibility tensor for an individual B-form DNA dodecamer, presumably as a result of either cooperativity in the alignment or transient stacking in the concentrated solution. In both myoglobin and the DNA dodecamer, changes of several hertz in one-bond dipolar coupling between low- and high-field measurements were reported, corresponding to alignment factors on the order of 10^{-4} . Much smaller effects were observed for a small diamagnetic model protein, ubiquitin, where the largest dipolar contribution to the change in ^1H – ^{15}N splitting between 360 and 600 MHz was only 0.2 Hz.²⁷ By choosing a more favorable system, where a small zinc-finger DNA-binding protein is complexed with a 16-base pair DNA fragment, changes in ^1H – ^{15}N splitting between 500 and 750 MHz as large as 2 Hz could be observed in the protein.²⁸ Although quite small, these numbers were used to recalculate the structure of this previously determined complex, and results demonstrated that dipolar couplings can considerably improve the accuracy of the structure. Initially, this improvement manifested itself by better local geometry, as evidenced by a twofold reduction of residues outside the most favored region of the Ramachandran map.²⁸ The dipolar couplings also resulted in a rigid-body rotation of a turn region, extruding from the globular part of the protein and not connected by long-range NOEs. This rotation was found to be in agreement with experimentally observed minute changes in ^{15}N chemical shift with field strength, resulting from incompletely averaged ^{15}N chemical shift anisotropy.²⁹ Although the shift in atomic coordinates of this turn region upon inclusion of the dipolar couplings was only a few angstroms, this work demonstrated that the global information contained in dipolar couplings indeed can be used to increase the accuracy of NMR structures.

- ¹³ D. Sikoff and D. A. Case, *Prog. Nucl. Magn. Reson. Spectrosc.* **32**, 165 (1998).
- ¹⁴ D. S. Wishart, B. D. Sykes, and F. M. Richards, *J. Mol. Biol.* **222**, 311 (1991).
- ¹⁵ S. Spelta and A. Bax, *J. Am. Chem. Soc.* **113**, 5490 (1991).
- ¹⁶ J. Kuszenski, J. Qin, A. M. Gronenborn, and G. M. Clore, *J. Magn. Reson. Ser. B* **106**, 92 (1995).
- ¹⁷ G. Cornilescu, F. Delaglio, and A. Bax, *J. Biomol. NMR* **13**, 289 (1999).
- ¹⁸ L. Banci, I. Bertini, G. G. Saveliani, A. Romagnoli, P. Turano, M. A. Cremomini, C. Luchinat, and H. B. Gray, *Prot. Struct. Funct. Genet.* **29**, 68 (1997).
- ¹⁹ M. Geochin, *J. Biomol. NMR* **12**, 243 (1998).
- ²⁰ J. Boisbouvier, P. Gijs, M. Blackledge, B. Brutscher, and D. Marion, *J. Am. Chem. Soc.* **121**, 7700 (1999).
- ²¹ A. Saupe, *Angew. Chem., Int. Ed. Engl.* **7**, 97 (1968).
- ²² J. W. Emsley, ed., "Liquid Crystals: General Considerations," Vol. 4 of "Encyclopedia of Nuclear Magnetic Resonance" (D. M. Grant and R. K. Harris, eds.), Wiley, Chichester, UK, 1996.
- ²³ C. Gayathra, A. A. Bothner-By, P. C. M. van Zijl, and C. MacLean, *Chem. Phys. Lett.* **87**, 192 (1982).
- ²⁴ A. A. Bothner-By, ed., "Magnetic Field Induced Alignment of Molecules" Vol. 5 of "Encyclopedia of Nuclear Magnetic Resonance" (D. M. Grant and R. K. Harris, eds.), Wiley, Chichester, UK, 1996.
- ²⁵ J. R. Tolman, J. M. Flanagan, M. A. Kennedy, and J. H. Prestegard, *Proc. Natl. Acad. Sci. U.S.A.* **92**, 9279 (1995).
- ²⁶ H. C. Kung, K. Y. W. IggorGoljer, and P. H. Bolton, *J. Magn. Res. Ser. B* **109**, 323 (1995).
- ²⁷ N. Tjandra, S. Grzesiek, and A. Bax, *J. Am. Chem. Soc.* **118**, 6264 (1996).
- ²⁸ N. Tjandra, J. G. Onichinski, A. M. Gronenborn, G. M. Clore, and A. Bax, *Nat. Struct. Biol.* **4**, 732 (1997).
- ²⁹ M. Ottinger, N. Tjandra, and A. Bax, *J. Am. Chem. Soc.* **119**, 9825 (1997).

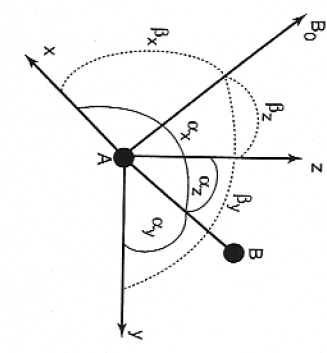


FIG. 1. Definition of the angles α_x , α_y , and α_z between an internuclear vector, \mathbf{r}_{AB} , and the molecular coordinate frame. The time-dependent angles β_x , β_y , and β_z define the orientation of the magnetic field relative to the x , y , and z axes of the molecular coordinate frame.

2.1. Rigid Molecules

If the molecule is rigid, the orientation of the internuclear vector, \mathbf{r}_{AB} , in an arbitrary molecular coordinate system can be described by the angles α_x , α_y , and α_z between the vector and the x , y , and z axes of the coordinate system. The angles β_x , β_y , and β_z define the instantaneous orientations of each of these axes relative to the static magnetic field (Fig. 1).

With $\cos \theta$ being the scalar product between a unit vector in the internuclear direction and a unit vector parallel to B_0 , $P_2(\cos \theta)$ can be rewritten as:

$$\langle P_2(\cos \theta) \rangle = \frac{3}{2} (\cos \beta_x \cos \alpha_x + \cos \beta_y \cos \alpha_y$$

$$+ \cos \beta_z \cos \alpha_z)^2 - \frac{1}{2} \quad (2a)$$

With $C_i = \cos \beta_i$ and $c_i = \cos \alpha_i$, this can be rewritten as

$$\begin{aligned} \langle P_2(\cos \theta) \rangle &= \frac{3}{2} [(\langle C_x \rangle^2 c_x^2 + \langle C_y \rangle^2 c_y^2 + \langle C_z \rangle^2 c_z^2 \\ &+ 2\langle C_x C_y \rangle c_x c_y + 2\langle C_x C_z \rangle c_x c_z \\ &+ 2\langle C_y C_z \rangle c_y c_z] - \frac{1}{2} \end{aligned} \quad (2b)$$

By writing $S_{ij} = \frac{3}{2}\langle C_i C_j \rangle - \frac{1}{2} \delta_{ij}$, where δ_{ij} is the Kronecker delta function, we obtain

$$\langle P_2(\cos \theta) \rangle = \sum_{ij=(x,y,z)} S_{ij} \cos \alpha_i \cos \alpha_j \quad (2c)$$

The 3×3 matrix S is commonly referred to as the Saupe matrix, the Saupe order matrix, or simply the order matrix. As $\langle C_x \rangle^2 + \langle C_y \rangle^2 + \langle C_z \rangle^2 = 1$, the matrix S is traceless, and with $\langle C_i C_j \rangle = \langle C_j C_i \rangle$, S is also symmetric and therefore contains only five independent elements.

If the structure of the molecule is known, i.e., $\cos \alpha_i$ factors in Eq. (2c) are known, the five independent elements of this matrix generally can be solved provided that dipolar couplings for at least five internuclear vectors are available. However, if any pair of internuclear vectors is parallel, and for other special cases such as a set that includes three mutually orthogonal interactions, more measured couplings are required. For macromolecules, many more dipolar couplings are frequently measured, and S is overdetermined. Its elements are then best determined using singular value decomposition.^{37,38}

The order matrix is real and symmetric, and it therefore is always possible to define a molecular axis system where S becomes diagonal. As will become clear below, in a number of applications it can be advantageous to work in this principal axis frame, where Eq. (2b) now simplifies to

$$D^{AB}(\alpha_x, \alpha_y, \alpha_z) = \frac{3}{2} D^{AB} \left\{ [\langle C_x \rangle^2 c_x^2 + \langle C_y \rangle^2 c_y^2 + \langle C_z \rangle^2 c_z^2] - 1 \right\} \quad (3a)$$

where $\langle C_i \rangle^2$ corresponds to the probability of finding the i th axis parallel to the magnetic field. Only the relative differences in the $\langle C_i \rangle^2$ values contribute to the residual dipolar coupling. So, writing $\langle C_i \rangle^2 = \frac{1}{3} + A_{ii}$, Eq. (3a) can be expressed in polar coordinates $\theta = \alpha_z$; $c_z = \cos \theta$; $c_x = \sin \theta \cos \phi$; $c_y = \sin \theta \sin \phi$ to yield

$$D^{AB}(\theta, \phi) = \frac{3}{2} D^{AB} [\cos^2 \theta A_{zz} + \sin^2 \theta \cos^2 \phi A_{xx} + \sin^2 \theta \sin^2 \phi A_{yy}] \quad (3b)$$

Defining $|A_{zz}| > |A_{yy}| > |A_{xx}|$ and using $A_{yy} + A_{xx} = -A_{zz}$; $2 \sin^2 \phi = 1 - \cos 2\phi$; and $2 \cos^2 \phi = 1 + \cos 2\phi$, this can be rewritten as

$$D^{AB}(\theta, \phi) = \frac{3}{2} D^{AB} \left[P_2(\cos \theta) A_{zz} + \frac{1}{2} \sin^2 \theta \cos 2\phi (A_{xx} - A_{yy}) \right] \quad (3c)$$

Defining an axial component of the alignment tensor $A_a = \frac{3}{2} A_{zz}$, and a rhombic component, $A_r = (A_{xx} - A_{yy})$ then results in

$$D^{AB}(\theta, \phi) = D^{AB} \left[P_2(\cos \theta) A_a + \frac{3}{4} A_r \sin^2 \theta \cos 2\phi \right] \quad (3d)$$

Note that the maximum value for $\langle C_i \rangle^2$ is 1, i.e., the maximum for A_{zz} equals $2/3$, and the maximum value for A_a becomes 1 when the z axis of the principal alignment tensor becomes fully aligned with the static field. In practice, the dilute liquid crystal work discussed in this chapter concerns A_a values on the order of 10^{-3} . Equation (3d) is sometimes rewritten as

$$D^{AB}(\theta, \phi) = D_a^{AB} \left[(3 \cos^2 \theta - 1) + \frac{3}{2} R \sin^2 \theta \cos 2\phi \right] \quad (3e)$$

³⁷ J. A. Losonczi, M. Andrec, M. W. F. Fischer, and J. H. Prestegard, *J. Magn. Reson.*, **138**, 334 (1999).

³⁸ W. H. Press, S. A. Teukolsky, W. T. Vetterling, and B. P. Flannery, "Numerical Recipes in C: The Art of Scientific Computing," 2nd ed. Cambridge University Press, Cambridge, UK, 1992.

where $D_{\text{a}}^{\text{AB}} = 1/2D_{\text{max}}^{\text{AB}}$, A_{a} is referred to as the magnitude of the residual dipolar coupling tensor, frequently normalized to the N–H dipolar interaction, and $R = A_{\text{r}}/A_{\text{a}}$ is the rhombicity.

2.2. Flexible Molecules

Above, the assumption of a rigid molecule was used. Clearly, this is an oversimplification for proteins where a substantial degree of internal dynamics is invariably present. First, the vibrational averaging of the internuclear distance needs to be considered. If this vibration is not coupled with librational motion, r^{-3} in Eq. (1b) may simply be replaced by $\langle r \rangle^{-3}$.

Provided that the shape (and charge distribution) of the molecule is not strongly influenced by the internal dynamics, the analysis of other motions remains tractable. For example, when the internuclear vector rotates on the surface of a cone with semiangle Ψ around its average orientation, the dipolar coupling is reduced by scaling by a factor $\cos \Psi(1 + \cos \Psi)/2$. This is directly equivalent to the order parameter,

$$S_{\text{cone}} = \cos \Psi(1 + \cos \Psi)/2 \quad (4)$$

commonly used in relaxation analysis.³⁹ In relaxation data analysis, typical values for the generalized order parameter S^2 for backbone bond vectors are on the order of 0.8–0.9. For the case of axially symmetric internal motion, the dipolar coupling therefore scales with the square root of the S^2 order parameter observed in relaxation studies.

For the case of nonaxially symmetric motion, such as a two- or three-site jump model where a side chain undergoes rotameric averaging, the observed dipolar coupling corresponds to the weighted sum of the individual conformers. In favorable cases, where the density of measured dipolar couplings exceeds the degrees of freedom available in the fit, dipolar couplings may become useful for analysis of internal molecular motions.

In cases where the shape of the molecule is affected by the internal motion, the alignment tensor itself becomes time-dependent. In the simplest case, where the molecule jumps between N different conformations one obtains for one-bond interactions:

$$D^{\text{AB}} = D_{\text{max}}^{\text{AB}} \sum_{k=1, \dots, N} F^k \sum_{i, j=[x, y, z]} S_{ij}^k \cos \phi_i^k \cos \phi_j^k \quad (5)$$

where F_k is the population of conformer k , ϕ_i^k refers to the angle in its molecular axis system, and S_{ij}^k refers to its S_{ij} Saupe matrix element. Usually, insufficient experimental dipolar couplings will be available to determine the individual conformers and their populations. Much work has focused on interpretation of

TABLE I
MAGNITUDE OF DIPOLEAR COUPLINGS RELATIVE TO ${}^1D_{\text{NH}}$

Parameter	X-ray ^a	NMR ^b
${}^1D_{\text{CaHs}}$	2.02	2.08
${}^1D_{\text{CaC'}}$	0.198	0.198
${}^1D_{\text{CN}}$	0.121	0.120
${}^2D_{\text{CHN}}$	0.319	0.300
${}^1D_{\text{CH3}}$	0.628 ^c	0.628 ^c

^a Optimized by fitting experimental couplings to ubiquitin X-ray structure.³⁷

^b Values that result in the lowest energy NMR structure ubiquitin, with best fit to ${}^{13}\text{C}'$ CSA X-ray structure.¹³⁸

^c Values obtained by comparison of ${}^1D_{\text{CH3}}$ and ${}^1D_{\text{CC}}$,⁶³ using ${}^1D_{\text{CC}} = {}^1D_{\text{CaC'}}$.

liquid crystal NMR spectra of strongly aligned flexible small molecules, where an abundance of long-range ${}^1\text{H}$ – ${}^1\text{H}$ and ${}^1\text{H}$ – ${}^{13}\text{C}$ dipolar couplings can frequently be measured.^{40,41} In proteins, it should be possible to evaluate populations of conformers that are in rapid conformational exchange, provided accurate structures for the individual conformers are available.

2.3. Estimate for Alignment Tensor

When working with a molecule of unknown structure, the above described singular value decomposition approach for determining the order matrix is not applicable. However, as briefly discussed below, a reasonable estimate for the principal components of the alignment tensor can be obtained from the range and distribution of observed dipolar couplings.

First, it is convenient to normalize all observed one-bond and two-bond dipolar couplings to, for example, the N–H dipolar coupling, by multiplying the observed P–Q dipolar coupling by $(\gamma_N \gamma_H r^3)/(r_P \gamma_Q r^3)$. Empirically determined optimum scaling factors are listed in Table I. In the absence of measurement error in the dipolar couplings, the bond vector with the largest absolute value for the normalized dipolar coupling provides a lower limit for $2D_{\text{a}}^{\text{NH}}$ in Eq. (3e). Similarly, an estimate for the rhombicity R in Eq. (3e) can be obtained from the dipolar coupling value, D_{opposite} , with the other extreme value (negative for $D_{\text{a}}^{\text{NH}} > 0$; positive for $D_{\text{a}}^{\text{NH}} < 0$). The value of R itself, defined in this manner, is always positive and follows from $D_{\text{opposite}} = -D_{\text{NH}}^{\text{a}}[1 + 3/2R]$, or

$$R = -\frac{2}{3}[1 + (D_{\text{opposite}}/D_{\text{a}}^{\text{NH}})] \quad (6)$$

⁴⁰ M. Gochin, A. Pines, M. E. Rosen, S. P. Rucker, and C. Schmidt, *Mol. Phys.*, **69**, 671 (1990).

⁴¹ J. W. Emsley, E. K. Foord, and J. C. Lindon, *J. Chem. Soc., Perkin Trans. 2*, 1211 (1982).

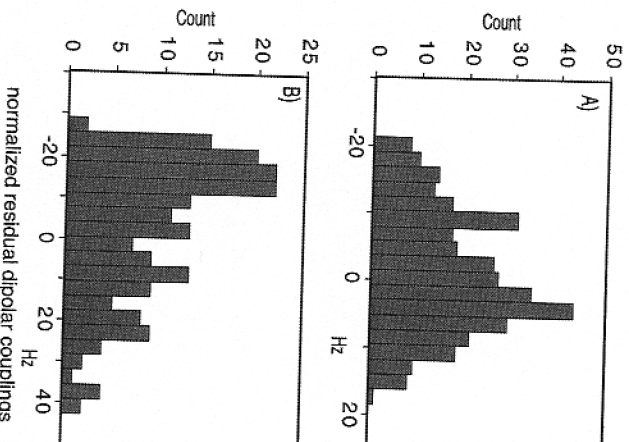


FIG. 2. Histogram of normalized dipolar couplings observed for the protein DiniI in (A) 5% (w/v) bicelle solution, 100 mM NaCl, and (B) a solution of 8 mg/ml Pfl phage and 150 mM NaCl. For (A) D_{NH} , $^1D_{\text{CaH}\alpha}$, $^2D_{\text{CHN}}$, $^1D_{\text{CN}}$, and $^1D_{\text{Cc}\alpha}$ dipolar couplings were measured; for (B) only D_{NH} , $^1D_{\text{CaH}\alpha}$, and $^1D_{\text{Cc}\alpha}$ dipolar couplings were used. From Ramirez *et al.*⁸⁶

This approach only uses the extreme values of the distribution of observed dipolar couplings. A more robust approach plots the histogram of the entire ensemble of normalized dipolar couplings.⁴² Figure 2 shows an example of two such histograms for the 81-residue protein DiniI. The histograms have been compiled from a nearly complete set of D_{NH} , $^1D_{\text{CaH}\alpha}$, $^1D_{\text{CN}}$, $^2D_{\text{CHN}}$, $^1D_{\text{Cc}\alpha}$ couplings, recorded in a bicelle medium, and a smaller set of couplings in phage medium.

It can be shown that for a uniform distribution of bond vectors, such a histogram will resemble the solid-state powder pattern observed for chemical shift anisotropy. In the present case, the singularities in the powder pattern correspond to D_{NH}^{zz} , D_{NH}^{xx} , and D_{NH}^{yy} , with the condition that $D_{\text{NH}}^{zz} + D_{\text{NH}}^{xx} + D_{\text{NH}}^{yy} = 0$. The relation between the powder pattern singularities D_{NH}^{zz} , D_{NH}^{xx} , D_{NH}^{yy} , and the parameters D_{a}^{NH} and R is given by⁴²:

$$D_{zz}^{\text{NH}} = 2D_{\text{a}}^{\text{NH}} \quad (7a)$$

$$D_{yy}^{\text{NH}} = -D_{\text{a}}^{\text{NH}}(1 + 1.5R) \quad (7b)$$

$$D_{xx}^{\text{NH}} = -D_{\text{a}}^{\text{NH}}(1 - 1.5R) \quad (7c)$$

If outliers appear to be present in the histogram, it is worthwhile to check the origin of these extreme dipolar couplings. They may correspond to $^1D_{\text{C}\beta\gamma}$, $^2D_{\text{C}\beta\gamma}$, or $^1D_{\text{C}\alpha\beta}$ couplings derived from weak or partially overlapping correlations. As a result of the large normalization constant, they can have substantial experimental error, and therefore should not be used.

3. Measurement of Dipolar Couplings

To date, measurement of dipolar couplings has focused primarily on one-bond interactions, which, as a result of their known internuclear distance, are readily interpreted in terms of orientation. Also, they are generally the easiest to measure. Two-bond interactions also have the benefit of a fixed internuclear distance, but owing to their larger separation, they are more difficult to measure at the same level of relative accuracy. New methods promise to make measurement of $^1\text{H}-^1\text{H}$ dipolar couplings more straightforward, and they may also become popular as structural restraints. Except for geminal $^1\text{H}-^1\text{H}$ interactions and pairs of protons in structural elements of fixed geometry, the interproton distance is an additional parameter influencing the dipolar coupling. This therefore results in a less direct relation between the value of the coupling and the orientation of the corresponding vector. However, structure calculation programs such as X-PLOR can readily deal with this additional complexity. Below, we briefly summarize some of the techniques that we have found to be most robust for measuring the various types of couplings, with particular emphasis on $^{15}\text{N}-^{13}\text{C}$ labeled proteins. With the exception of couplings between protons separated by more than three bonds, where the J coupling is usually negligible, the coupling observed in the liquid crystalline phase represents the sum of the scalar and dipolar contributions. Considerable variation in the scalar couplings frequently exists, making it necessary to measure the couplings both in the isotropic and aligned environment. Although, on the one hand this may be considered unfortunate because it doubles the number of experiments, variations in the isotropic $^1J_{\text{CaH}\alpha}$ and $^1J_{\text{C}\alpha\text{C}\beta}$ can yield useful angular restraint information,^{43,44} and J_{CN} is related to hydrogen bonding.⁴⁵

3.1. Accuracy of Measured Splitting

In the absence of any systematic line shape or phase distortions, the accuracy of a peak position is directly proportional to its signal-to-noise ratio, and inversely related to its line width.⁴⁶ Although the accuracy depends also on the shape of the time domain data, on the method used for peak position determination, and on the digital resolution, a reasonable approximation for the root-mean-square

⁴³ G. W. Vuister, F. Delaglio, and A. Bax, *J. Am. Chem. Soc.* **114**, 9674 (1992).

⁴⁴ G. Comitescu, A. Bax, and D. A. Case, *J. Am. Chem. Soc.* **122**, 2168 (2000).

⁴⁵ N. Juranic, P. K. Illich, and S. Macura, *J. Am. Chem. Soc.* **117**, 405 (1995).

⁴⁶ G. Kontaxis, G. M. Clore, and A. Bax, *J. Magn. Reson.* **143**, 184 (2000).

uncertainty, ΔJ , in a measured splitting for a well-resolved, undistorted, pure phase or pure antiphase doublet one can use:

$$\Delta J = LW/SN \quad (8)$$

where LW is the line width at half height (in the dimension where the splitting is being measured), and SN is the signal-to-noise ratio. Note that Eq. (8) provides a lower limit for the accuracy of the measurement, as other distortions such as partial overlap or imperfect phasing can also contribute.

3.2. Measurement of $^1J_{HN}$

One-bond $^1D_{NH}$ dipolar coupling were the first ones to be measured in a weakly oriented protein, simply by recording a 1H - ^{15}N HSQC spectrum without the regular 1H 180° decoupling pulse applied at the midpoint of the t_1 evolution period. Transverse relaxation is considerably slower in the ^{15}N dimension compared to the 1H dimension, and measurement in the indirect ^{15}N dimension is therefore preferred over measurement in the 1H dimension. However, the spectral crowding doubles when HSQC spectra are recorded without decoupling, typically resulting in an unacceptable degree of resonance overlap.

An interesting solution to solving this overcrowding problem is to record the HSQC spectrum in such a way that the fraction of the ^{15}N magnetization doublet components that are in-phase and antiphase at the end of a constant-time (CT) ^{15}N evolution period are stored separately.⁴⁷ This experiment is best suited for measurement of small dipolar couplings ($<(2CT)^{-1}$), although with minor adaptation it can be converted to measurement of dipolar couplings of any size. Another method that can yield very accurate values for $^1J_{HN}$ measures the intensity modulation of a regular 2D HSQC as a function of a dephasing delay, and this method was used to detect the minute changes (<0.2 Hz) in the $^1J_{HN}$ splitting as a function of field strength in the diamagnetic protein ubiquitin.²⁷

In liquid crystalline media the ^{15}N - 1H dipolar coupling is typically many hertz, and any method that yields an accuracy of ca 1 Hz is adequate for most practical purposes. A conceptually very simple method for measuring $^1J_{HN}$ separates the F_1 -coupled HSQC into two separate subspectra. The pulse scheme of Fig. 3 is executed n an interleaved manner, once with the additional dephasing delay at the beginning of t_1 , and once without. These two pulse schemes result in antiphase and in-phase $^1_1^{15}N$ - 1H doublets, with the antiphase spectrum typically being 10–20% weaker as a result of the additional delay and imperfect 180° pulses. After scaling up the inphase spectrum by this 10–20%, the difference with the in-phase spectrum only yields the downfield component, whereas the sum yields only the upfield

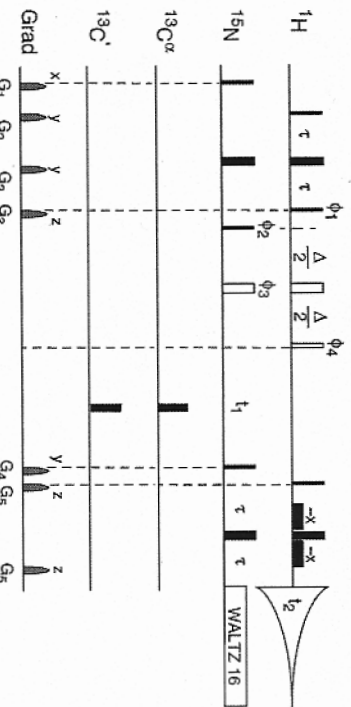


FIG. 3. Pulse scheme of the IPAP ^{15}N - 1H HSQC experiment. Narrow and wide pulses correspond to 90 and 180° flip angles, respectively, with phase x , unless indicated. The $\Delta/2$ -180°($^1H/^{15}N$)- $\Delta/2$ -90° sequence (open pulses) is only used in the experiment for generating the antiphase (AP) spectrum and is omitted for generating the in-phase (IP) spectrum. IP and AP spectra are recorded in an interleaved manner and, with the Bruker software version used (UXNMR 2.2), no gradients could be used around the 180° ϕ_3 ^{15}N pulse. The low power 90°- π pulses surrounding the final 1H 180° pulse are part of the WATERGATE solvent suppression scheme.¹⁹ $^{13}C'$ and ^{13}C 180° pulses are applied to decouple ^{13}C from ^{15}N during t_1 . These pulses are applied sequentially and have durations of $\sqrt{3}/(2\Delta\delta)$ s (where $\Delta\delta$ is the frequency difference between the centers of the $^{13}C^\alpha$ and $^{13}C'$ regions). Delay durations: $\tau = 2.5$ ms; $\Delta = 5.3$ ms. All gradients are sine-bell shaped with 25 G/cm at their center. Gradient durations: $G_{1,2,3,4,5} = 2, 0.4, 2, 1, 0.4$ ms. Phase cycling: $\phi_1 = -y, y; \phi_2 = 2(x), 2(-x)$ for IP; $\phi_2 = 2(-y), 2(y)$ for AP; $\phi_3 = 4(x), 4(y), 4(-x), 4(-y); \phi_4 = 8(x), 8(-x); \text{Receiver} = x, 2(-x), x$ for IP; $\text{Receiver} = x, 2(-x), x, -x, 2(x), -x$ for AP. Quadrature detection in the t_1 dimension is obtained by altering ϕ_2 (IP) or ϕ_2 and ϕ_3 simultaneously (AP) in the usual States-TPII manner. From Ottinger *et al.*⁴⁸

component (Fig. 4). This approach is referred to as IPAP (for in-phase and antiphase)⁴⁸ and is conceptually similar to the earlier so-called S³E method,^{49,50} but IPAP is less sensitive to deviations from uniformity of the one-bond interactions.

For larger proteins, even the regular HSQC spectrum, and thereby also the IPAP-HSQC spectrum, may exhibit too much overlap. It then becomes advantageous to obtain the $^1J_{HN}$ from a 3D HNCO spectrum, recorded without 1H dephasing in the ^{15}N dimension. When adding the sensitivity enhancement feature to this pulse sequence,⁵¹ special care must be taken that the doublets are purely absorptive in the ^{15}N dimension as even small phase errors can result in considerable changes in the measured splittings.

For larger proteins, in particular when the rotational correlation time exceeds 15 ns, a second complication is that the upfield ^{15}N - 1H doublet component is

⁴⁸ M. Ottinger, F. Delaglio, and A. Bax, *J. Magn. Reson.* **131**, 373 (1998).

⁴⁹ A. Meissner, J. O. Düns, and O. W. Sørensen, *J. Biomol. NMR* **10**, 89 (1997).

⁵⁰ A. Meissner, T. Schulte-Herbrüggen, and O. W. Sørensen, *J. Am. Chem. Soc.* **120**, 3803 (1998).

⁵¹ L. E. Kay, G. Y. Xu, and T. Yamazaki, *J. Magn. Reson. Ser. A* **109**, 129 (1994).

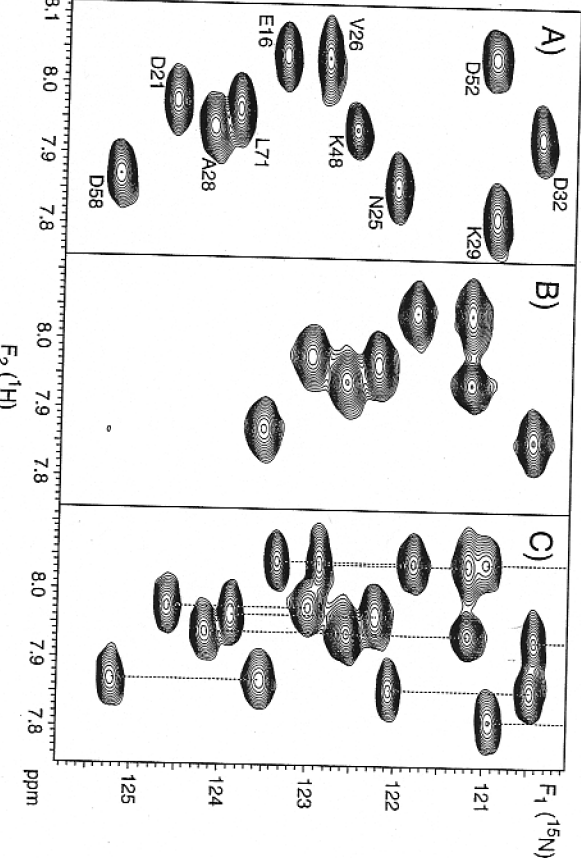


Fig. 4. Regions of the ubiquitin ^1H - ^{15}N HSQC spectrum recorded in the liquid crystalline phase. (A) Downfield and (B) upfield doublet components of the IPAP-HSQC spectrum, obtained by (A) subtracting and (B) adding the in-phase and antiphase signals obtained with the pulse scheme of Fig. 1, using a scaling factor of 1.11 for the antiphase signals. For comparison, (C) shows the regular ^1H -coupled ^1H - ^{15}N HSQC spectrum. Note that the upfield doublet components are broader than the downfield components as a result of relaxation interference.⁵² (From M. Ortiger, F. Delaglio, and A. Bax, *J. Magn. Reson.*, **131**, 373 (1998).

broadened and thereby weakened as a result of interference between the ^{15}N - ^1H dipolar coupling and ^{15}N chemical shift anisotropy relaxation mechanisms.⁵² This provided the impetus for the development of the TROSY method, which selectively detects only the downfield ^{15}N -{ ^1H } doublet component (correlated to the narrower upfield ^1H -{ ^{15}N } doublet component).⁵³ Because of the weakness of the broad, upfield ^{15}N -{ ^1H } doublet components, it may be advantageous to extract the $^1J_{\text{NH}}$ coupling from the difference in ^{15}N frequency between the TROSY component and a ^1H -decoupled spectrum, provided special care is taken that the spectra are recorded at exactly the same temperature.⁴⁶ As in this method $^1J_{\text{NH}}$ is derived from doubling the frequency difference between the decoupled and TROSY line positions, errors in the measurement are also doubled. Two closely related methods have been proposed that simply scale the position of the broad upfield ^{15}N -{ ^1H } doublet component in the 3D HNCO spectrum, but retain some of the sensitivity

advantage of the regular TROSY version of this experiment.^{46,54} These methods are preferred for the study of larger proteins.

3.3. Measurement of $^1J_{\text{CC}\alpha}$

Because of the longer internuclear distance and the lower product of the gyromagnetic ratios involved, the $^1J_{\text{CC}\alpha}$ coupling is inherently 5 times smaller than the one-bond ^1H - ^{15}N coupling (Table I). In order to obtain meaningful information, it therefore is necessary to measure this coupling at higher accuracy. There are two ways to measure $^1J_{\text{CC}\alpha}$: observation of the C^α or of the C' resonance in the absence of decoupling the nonobserved spin. It is also possible to "transform" the $^1J_{\text{CC}\alpha}$ splitting such that it appears in the ^{15}N dimension of the spectrum,⁵⁵ but in essence this experiment falls into the C' -observed half of experiments as the line width in the dimension in which the splitting appears is a function of the C' transverse relaxation rate. For protonated proteins, the $\text{C}'T_2$ is invariably much longer than the $\text{C}^\alpha T_2$, favoring detection of C' for most accurate measurement of $^1J_{\text{CC}\alpha}$. For perdeuterated proteins, detection of $^{13}\text{C}^\alpha$ in the presence of ^2H and $^{13}\text{C}^\beta$ decoupling can yield higher resolution, particularly at higher fields. To this extent, either an HNCA or an HN(CO)CA experiment or a TROSY version thereof may be used.

In most cases, for protonated proteins the most effective method for measurement of $^1J_{\text{CC}\alpha}$ is simply the recording of a 3D HNCO spectrum, where the C^α pulse, normally applied at the midpoint of the $^{13}\text{C}'$ evolution period, is omitted.⁵⁶ The HNCO spectrum is among the best resolved triple resonance experiments, and the twofold increase in the number of resonances relative to the $^{13}\text{C}^\alpha$ -decoupled spectrum is generally not much of a problem. The $^{13}\text{C}'$ transverse relaxation rate is dominated by its chemical shift anisotropy, and $^{13}\text{C}'$ line widths at 600 MHz are about 25% larger than at 500 MHz ^1H frequency. In our experience, it is therefore preferable to measure the $^1J_{\text{CC}\alpha}$ splitting at a relatively low magnetic field strength. This requirement is, however, somewhat in conflict with the requirement for a high field when the TROSY version of the HNCO experiment is used,^{54,55} which lengthens the ^{15}N transverse relaxation time with increasing magnetic field strength. Nevertheless, a field strength of ca 11 tesla remains a close-to-optimal compromise.

3.4. Measurement of $^1J_{\text{CN}}$ and $^2J_{\text{CHN}}$

Dipolar couplings across the peptide bond between $^{15}\text{N}_i$ and $^{13}\text{C}_{i-1}$ are inherently 8.3 times weaker than $^1J_{\text{DNH}}$ (Table I). Therefore, accuracy of their

⁵² M. Goldman, *J. Magn. Reson.*, **60**, 437 (1984).

⁵³ K. Pervushin, R. Riek, G. Wider, and K. Wuthrich, *Proc. Natl. Acad. Sci. U.S.A.*, **94**, 12366 (1997).

⁵⁴ D. W. Yang, R. A. Venters, G. A. Mueller, W. Y. Choy, and L. E. Kay, *J. Biomol. NMR* **14**, 333 (1999).

⁵⁵ P. Perini and A. Annala, *J. Biomol. NMR* **16**, 221 (2000).

⁵⁶ S. Grzesiek and A. Bax, *J. Magn. Reson.*, **96**, 432 (1992).

measurement is critical for making optimal use of these small couplings in structure determination. Owing to the favorable relaxation properties of ^{15}N , especially when selecting the downfield ^{15}N doublet component, the $^1J_{\text{CN}}$ coupling is detected through the ^{15}N and not the $^{13}\text{C}'$ nucleus. The simplest method just records a 2D HSQC on the $^{13}\text{C}'/\text{H}$ doubly labeled protein, and inserts a $^{13}\text{C}^\alpha$ but not a $^{13}\text{C}'$ 180° decoupling pulse at the midpoint of ^{15}N evolution.⁵⁷ The resulting doublet in the ^{15}N dimension corresponds to $^1J_{\text{CN}}$. Interestingly, the detected amide proton is also coupled to $^{13}\text{C}'$ (which has not changed its spin state during or after ^{15}N evolution). Therefore, the two doublet components are also displaced relative to one another by the $^2J_{\text{CHN}}$ coupling in the $^1\text{H}'$ dimension. Although normally this splitting would be very difficult to resolve because the $^1\text{H}'$ line width is typically much larger than the $^2J_{\text{CHN}}$ coupling, the E.COSY principle⁵⁸ effectively separates the two $^1\text{H}'-\{^{13}\text{C}'\}$ doublet components (Fig. 5).

For small and medium-size protonated proteins, with a rotational correlation time shorter than about 10 ns, the cpd-decoupled semiconstant time scheme of Fig. 6A is the most effective 2D scheme for simultaneous measurement of $^1J_{\text{CN}}$ and $^2J_{\text{CHN}}$. For larger proteins, or for perdeuterated proteins, the $^{13}\text{C}'$ -coupled TROSY $^{15}\text{N}-\text{H}$ correlation is preferred (Fig. 6B). Alternatively, an IPAP-HSQC spectrum without $^{13}\text{C}'$ decoupling can be recorded to simultaneously obtain $^1J_{\text{NH}}$, $^1J_{\text{CN}}$, and $^2J_{\text{CHN}}$ (Fig. 5).

The increase in spectral crowding resulting from the $^1J_{\text{CN}}$ splittings, in addition to the normally already very crowded nature of the HSQC spectrum, can make it desirable to again go to a 3D, HNCO-based detection scheme.^{46,54,55} An interesting alternative pulse sequence, which is based on the principle of quantitative J correlation,⁴ derives $^1J_{\text{CN}}$ from the relative intensities of two interleaved 3D TROSY-HNCO spectra.⁶⁰ In one experiment (reference spectrum) the pulse scheme uses optimal $^{15}\text{N}-\{^{13}\text{C}'\}$ dephasing of 33 ms, whereas in the second experiment (attenuated spectrum) the dephasing delay is set near the null condition (66 ms). The relative intensities in these two spectra give a very accurate measure for $^1J_{\text{CN}}$, and permit $^1D_{\text{CN}}$ to be derived at an accuracy that is a fraction of a hertz, provided the signal to noise in the reference spectrum exceeds 20 : 1. A drawback with this method is that it only provides $^1J_{\text{CN}}$ and not $^2J_{\text{CHN}}$. On the other hand, the $\text{C}'-\text{H}'$ vector falls in between the $\text{C}'-\text{N}$ and $\text{N}-\text{H}$ orientations, and differs from the $\text{C}'-\text{N}$ vector by only 25°. Considering that for a known planar geometry such as a peptide bond, three dipolar couplings fully determine its orientation (except for 8-fold ambiguity), measurement of $^2D_{\text{CHN}}$ is less essential.

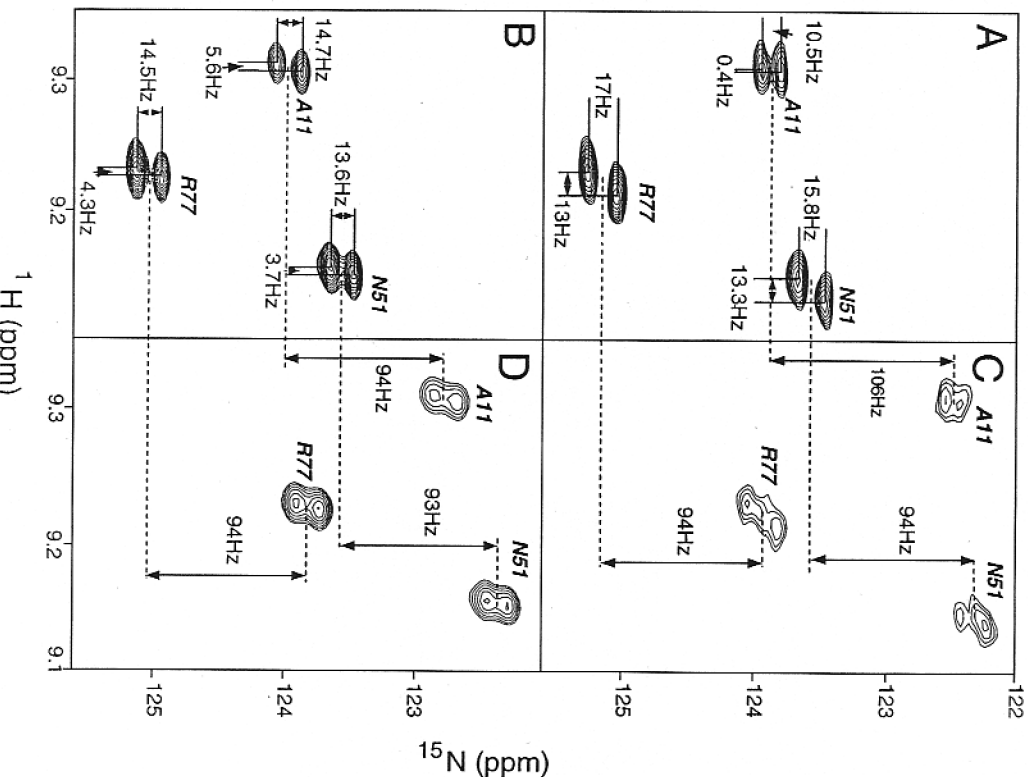


Fig. 5. Small sections of the IPAP- $^1\text{H}-^{15}\text{N}$ -HSQC spectrum of U-($^{15}\text{N}/^{13}\text{C}/^2\text{H}$) MAP30 protein (molecular mass 30 kDa), recorded at 750 MHz in the absence of $^{13}\text{C}'$ decoupling. (A and B) downfield $^{15}\text{N}-\{\text{H}\}$ doublet components and (C and D) upfield doublet components; (A and C) 0.15 mM MAP30 in bicelle medium and (B and D) in the isotropic phase. The small vertical splittings correspond to $^1J_{\text{CN}}$, small horizontal displacements to $^2J_{\text{CHN}}$, and vertical displacement between panels B and D to $^1J_{\text{NH}}$. Reprinted with permission from Wang *et al.*⁴⁰

⁵⁷ F. Delaglio, D. A. Torchia, and A. Bax, *J. Biomol. NMR* **1**, 439 (1991).

⁵⁸ C. Griesinger, O. W. Sørensen, and R. R. Ernst, *J. Magn. Reson.* **75**, 474 (1987).

⁵⁹ Deleted in proof.

⁶⁰ J. J. Choi, F. Delaglio, and A. Bax, *J. Biomol. NMR* **18**, 101 (2000).

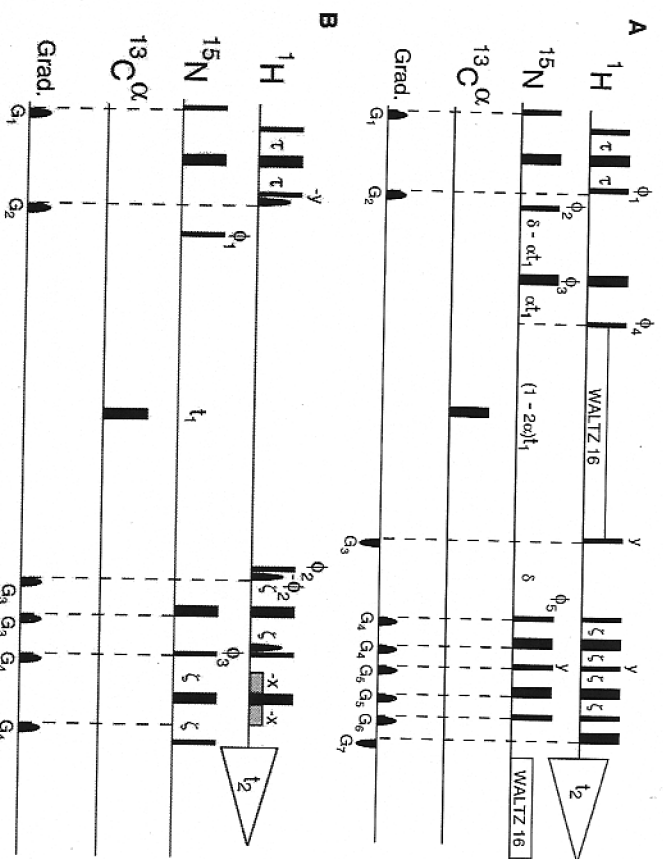


Fig. 6. Pulse schemes of (A) the CPD-decoupled, gradient-enhanced ^1H - ^{15}N -HSQC experiment, and (B) the ^1H - $^{13}\text{C}^\alpha$ -TRSY experiment⁴⁴⁵ for measurement of $^1\text{J}_{\text{cN}}$ and $^2\text{J}_{\text{cHN}}$ couplings. Narrow and wide pulses correspond to 90 and 180° flip angles, respectively, with phase x , unless indicated. All gradients are sine bell-shaped with 25 G/cm at their center. In pulse scheme A, the $^{13}\text{C}^\alpha$ 180° pulse applied during the t_1 evolution period to decouple $^{13}\text{C}^\alpha$ from the ^{15}N has a duration of $\sqrt{3}/(2\Delta\delta)$ s (where $\Delta\delta$ is the frequency difference between the centers of the $^{13}\text{C}^\alpha$ and $^{13}\text{C}'$ regions). For optimal $^{13}\text{C}^\alpha$ decoupling, this pulse is applied at time $t_1/2$ prior to the last ^{15}N 90° pulse. Delay durations: $\tau = 2.25$ ms; $\delta = 5.3$ ms; $\zeta = 2.67$ ms. The value α equals $\delta/t_{1,\max}$. Phase cycling: $\phi_1 = x, -y; \phi_2 = 2(x), 2(-x); \phi_3 = 4(x), 4(y), 4(-x), 4(-y); \phi_4 = 8(y), 8(-y); \phi_5 = x; \text{receiver} = x, 2(-x), x, -x, 2(x), -x$. Gradient durations: $G_{1,2,3,4,5,6,7} = 5, 1, 2, 2.705, 1.2, 1.1, 0.2, 0.075$ ms, with respective gradient axes: $-xz, xyz, z, x, y, z$. Rance-Kay quadrature detection¹⁴¹ in the t_1 dimension is obtained by changing the gradient G_3 polarity in concert with alternating phase ϕ_5 between x and $-x$. In pulse scheme B, the same 180° pulse was used to decouple the $^{13}\text{C}^\alpha$ from ^{15}N during the t_1 evolution period as in scheme A. Delay durations: $\tau = 2.25$ ms; $\zeta = 2.67$ ms (including the 2-ms sine-bell-shaped water flip back pulses). The low power 90° $_{-x}$ pulses surrounding the final ^1H 180° pulse are part of the WATERGATE scheme.¹³⁹ Phase cycling: $\phi_1 = x, y, -x, -y; \phi_2 = -y; \phi_3 = y; \text{receiver} = x, y, -x, -y$. Quadrature detection in the t_1 dimension is obtained by acquiring a second signal with $\phi_1 = -x, y, x, -y; \phi_2 = y; \phi_3 = -y; \text{rec} = x, 2(-x), x, -x, 2(x), -x$. Gradient durations: $t_{1,2,3,4} = 4, 1.4, 0.6$ and 0.4 ms, with respective gradient axes: x, xyz, xy, z . Gradient durations:

3.5. Measurement of $^1\text{J}_{\text{cH}\alpha}$

Although, in principle, $^1\text{J}_{\text{cH}\alpha}$ can be measured from a ^1H - ^{13}C 2D correlation spectrum, recorded in the absence of heteronuclear decoupling in either

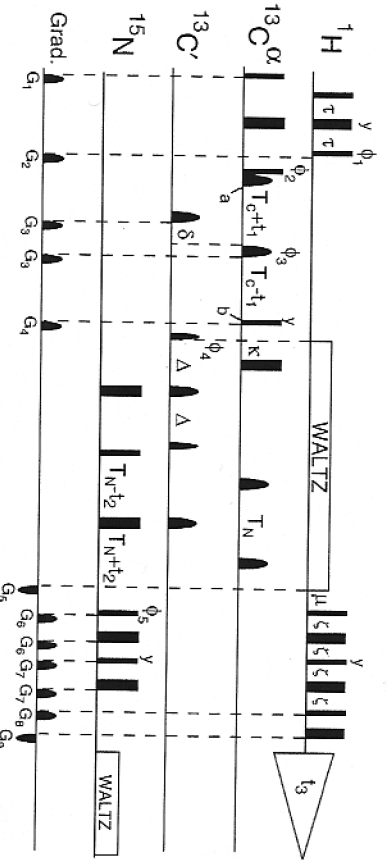


Fig. 7. Pulse sequence of the $^1\text{H}^\alpha$ -coupled (HA)CA(CO)NH experiment. Narrow and wide pulses correspond to flip angles of 90 and 180°, respectively. Pulses following the WALTZ ^1H decoupling yield gradient-enhanced $^1\text{H}^\alpha \rightarrow \text{H}^\alpha$ magnetization transfer. Shaped $^{13}\text{C}^\alpha$ pulses are of the hyperbolic secant type, with a squareness level of 3, and durations of 500 μs at 151 MHz ^{13}C frequency. The first shaped $^{13}\text{C}^\alpha$ pulse (time a) compensates for phase errors introduced by the second shaped $^{13}\text{C}^\alpha$ 180° pulse. $^{13}\text{C}^\alpha$ pulses have the shape of the center lobe of a $\sin x/x$ function, and durations of 180 μs . The RF phase of all pulses is x , unless indicated. Delay durations: $\tau = 1.4$ ms; $\zeta = 2.67$ ms; $T_c = 1.4$ ms; $T_N = 15$ ms; $\delta = 5.5$ ms; $\Delta = 13$ ms; $\kappa = 4.6$ ms; $\mu = 5.35$ ms. Phase cycling: $\phi_1 = y, -y; \phi_2 = x, y; \phi_3 = 2(x), 2(y); \phi_4 = 4(x), 4(-x); \text{rec} = x, 2(-x), x, -x, 2(x), -x$. Rance-Kay quadrature detection is used, alternating ϕ_5 between x and $-x$ in concert with the polarity of gradient G_5 .¹⁴¹ and t_1 quadrature is obtained by using States-TPII phase cycling of ϕ_2 . All gradients are sine-bell shaped, with 25 G/cm (10 G/cm for $G_{5,8,9}$) at their center. Gradient durations: $G_{1,2,3,4,5,6,7,8,9} = 4, 2, 1, 2.1, 2.705, 1.2, 1.1, 0.2, 0.075$ ms, with respective gradient axes: $xy, xy, xz, yz, z, x, y, z, z$.

the F_1 or F_2 dimension, the increase in spectral crowding frequently leads to unacceptable overlap for all but the smallest proteins. In practice, therefore, $^1\text{J}_{\text{cH}\alpha}$ is most commonly measured either from a series of J_{CH} -modulated HSQC spectra, simultaneous to measurement of side-chain J_{CH} couplings (see Section 3.6), or from a H^α -coupled HN(CO)CA or (HA)CA(CO)NH spectrum. This latter experiment makes it easy to decouple the $^1\text{J}_{\text{cH}\beta}$ coupling by using a constant-time $^{13}\text{C}^\alpha$ evolution period, and is therefore preferred when dealing with small or medium-size proteins. Its pulse sequence is shown in Fig. 7. The (HA)CA(CO)NH experiment, in the absence of ^1H decoupling in the C^α dimension, yields antiphase doublets from which $^1\text{J}_{\text{cH}\alpha}$ is easily measured (see Fig. 8). For Gly residues the observed antiphase “doublet” corresponds to the outer lines of its ^{13}C -{ H_2 } triplet, and the measured splitting represents the sum of $^1\text{J}_{\text{cH}\alpha\text{H}\alpha 2}$ and $^1\text{J}_{\text{cH}\alpha\text{H}\alpha 3}$.

Provided the Boltzmann $^{13}\text{C}^\alpha$ magnetization has been destroyed prior to the start of the pulse sequence, the relative intensities of the two doublet components are related to relaxation interference between the $^{13}\text{C}^\alpha$ CSA mechanism and the $^{13}\text{C}^\alpha$ - $^1\text{H}^\alpha$ dipolar coupling, which is related to the backbone torsion angles ϕ and ψ . Interestingly, the isotropic $^1\text{J}_{\text{cH}\alpha}$ coupling is also related to ϕ and Ψ and

this can result in high energy distorted sidechain conformations. A way around this is to impose the observed dipolar coupling as a lower bound for the true dipolar coupling.⁶¹ An even better way would be to evaluate for each site separately what the degree of side-chain mobility is by conducting the requisite relaxation experiments,⁶² but no studies have yet been reported that have combined these two sources of information.

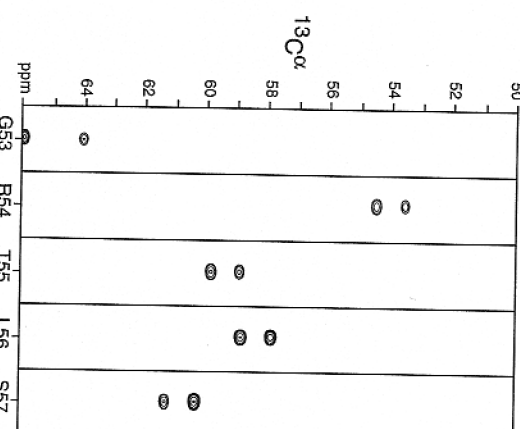


FIG. 8. Strips taken parallel to the F_1 axis of the $^{1\text{H}}\text{H}^{\alpha}$ -coupled (HA)CAC(CO)NH spectrum of ubiquitin, taken at the (F_2 , F_3) frequencies of the amides of Gly⁵³–Ser⁵⁷ of ubiquitin. The correlation of Gly-53 is folded in the F_1 dimension.

is particularly useful for identifying residues with positive ϕ angles.⁴³ Residues with $^{1\text{J}}_{\text{CaH}\alpha} < 137$ Hz have a positive ϕ angle; and residues in helical regions have larger $^{1\text{J}}_{\text{CaH}\alpha}$ values than in extended regions.

The intrinsic magnitude of $^{1\text{D}}_{\text{CH}}$ is twice that of $^{1\text{D}}_{\text{NH}}$ (Table I). Consequently, these dipolar couplings are the largest ones found in a protein and can have values exceeding 50 Hz. Even if their measurement is made at relatively low precision, say ± 5 Hz, these couplings are still very useful in structure determination. For this reason, it may not be essential to obtain the highest possible resolution in the $^{13}\text{C}^{\alpha}$ dimension of the 3D spectrum. If signal-to-noise is insufficient for obtaining a CT-(HA)CA(CO)NH spectrum, a H^{α} -coupled HN(CO)CA 3D spectrum with a 10 ms acquisition time in the C^{α} dimension typically yields $^{1\text{J}}_{\text{CaH}\alpha}$ couplings at sufficient accuracy, or a quantitative CB(CA)CONH scheme may be used.¹⁴³

3.6. Measurement of Side-Chain $^{1\text{J}}_{\text{CH}}$ Couplings

To date, most attention has focused on measurement of backbone-related dipolar couplings. However, dipolar couplings also are expected to become widely used for accurate determination of sidechain conformations. A problem here sometimes is that a significant fraction of the side chains are subject to rotameric averaging, which reduces the dipolar coupling relative to a static, single conformation. If the smaller dipolar coupling is imposed during structure calculation, as if it were rigid,

this can result in high energy distorted sidechain conformations. A way around this is to impose the observed dipolar coupling as a lower bound for the true dipolar coupling.⁶¹ An even better way would be to evaluate for each site separately what the degree of side-chain mobility is by conducting the requisite relaxation experiments,⁶² but no studies have yet been reported that have combined these two sources of information.

For small and medium-size proteins, an accurate way for extracting both backbone $^{1\text{J}}_{\text{CaH}\alpha}$ and side-chain $^{1\text{J}}_{\text{CH}}$ couplings is the recording of a set of CT-HSQC spectra, in which the $^{1\text{H}}$ 180° decoupling pulse is systematically shifted. The intensity modulation pattern observed in the fully decoupled CT-HSQC spectrum then provides an accurate measure for $^{1\text{J}}_{\text{CH}}$. For methylene groups, the modulation frequency corresponds to the sum of the two $^{1\text{J}}_{\text{CH}}$ couplings. Methyl group intensities are modulated by $^{1\text{J}}_{\text{CH}}$ and by $3 \times {^{1\text{J}}_{\text{CH}}}$, with amplitudes of the modulation having a ratio of approximately 1:3. As a result of the rapid rotation about the three-fold symmetry axis of the methyl group, the $^{1\text{D}}_{\text{CH}}$ dipolar coupling is scaled down by -0.31 relative to its static value.⁶³ For structure calculation purposes its value is most easily converted into a restraint for the C–C(H₃) orientation.

For larger proteins, the lower sensitivity and increased spectral overlap in a CT-HSQC spectrum frequently result in a relatively small fraction of residues for which the $^{1\text{J}}_{\text{CH}}$ coupling can be measured. As an alternative, spectra recorded with CCH-COSY or HCCH-COSY^{64–66} without decoupling in the detected dimension may be used for measurement of J_{CH} . An additional benefit of this approach is that for the case of nonequivalent methylene protons, both J_{CH} couplings can be measured separately. In favorable cases, the $^{1\text{H}}\text{H}$ – $^{1\text{H}}\text{H}$ multiplet structure in such spectra also permits measurement of $^{2\text{J}}_{\text{HH}}$.⁶⁷

A very elegant approach, which permits simultaneous measurement of both individual $^{1\text{J}}_{\text{CH}}$ methylene couplings, in addition to yielding a sign-sensitive value of $^{2\text{J}}_{\text{HH}}$, has been described by Griesinger and co-workers.⁶⁸ The experiment is referred to as SPTZE-HSQC and uses spin-state selective transfers to generate E.COSY type patterns for the heteronuclear cross multiplet. The experiment has only been described in a 2D manner, but can be extended to three dimensions. The experiment is particularly well suited for Gly $\text{C}^{\alpha\alpha}$ – $\text{H}^{\alpha\alpha}$ and $\text{H}^{\alpha 2}$ – $\text{H}^{\alpha 3}$ interactions. For side-chain carbons extra losses result from ^{13}C – ^{13}C coupling.

⁶¹ M. Omtjger, F. Delgelio, J. L. Marquardt, N. Tjandra, and A. Bax, *J. Magn. Reson.* **134**, 365 (1998).

⁶² D. W. Yang, A. Mittermaier, Y. K. Mok, and L. E. Kay, *J. Mol. Biol.* **276**, 939 (1998).

⁶³ M. Omtjger and A. Bax, *J. Am. Chem. Soc.* **121**, 4690 (1999).

⁶⁴ S. W. Fesik, H. L. Eaton, T. T. Olejniczak, and E. R. P. Zuiderweg, *J. Am. Chem. Soc.* **112**, 886 (1990).

⁶⁵ L. E. Kay, M. Ikura, and A. Bax, *J. Am. Chem. Soc.* **112**, 888 (1990).

⁶⁶ K. Gehring and I. Ekiel, *J. Magn. Reson.* **135**, 185 (1998).

⁶⁷ E. T. Olejniczak, R. P. Meadows, H. Wang, M. L. Cai, D. G. Nettesheim, and S. W. Fesik, *J. Am. Chem. Soc.* **121**, 9249 (1999).

⁶⁸ T. Carloniagno, W. Peti, and C. Griesinger, *J. Biomol. NMR* **17**, 99 (2000).

3.7. Measurement of ^1H - ^1H Couplings

The history of measuring ^1H - ^1H J couplings is particularly rich and has been reviewed in numerous places.^{5,6,69-71} The E.COSY approach, applied in either a homo- or heteronuclear manner, has proven particularly useful in this respect. However, relatively few of these methods have been used for measurement of ^1H - ^1H dipolar couplings. When oriented, ^1H - ^1H multiplet structure tends to become very complex as a result of the multitude of coupling partners any given proton experiences. However, in heteronuclear type E.COSY spectra this does not pose a serious problem, and the utility of triple resonance experiments for measurement of both the sign and magnitude of intraresidue and sequential J_{Hahn} couplings has been demonstrated in oriented media.⁷² Nevertheless, with some exceptions,^{73,74} such experiments tend to be less suitable for measurement of dipolar couplings that are spatially proximate but far apart in the covalent bond network.

Measurement of dipolar coupling between remote protons in a protein through dipolar coupling was first demonstrated using the HNHA technique,^{33,75} and some of the data obtained with this technique are shown in Fig. 9A. The magnitude of $|J_{\text{HH}} + D_{\text{HHL}}$ is derived from the diagonal to cross peak intensity ratio. The interresidue interactions seen in the spectrum are marked by dashed lines in the corresponding region of the protein (Fig. 9B). This molecular fragment is oriented such that the vertical axis corresponds to the z axis of the nearly axially symmetric alignment tensor. As expected, most of the interactions are either parallel or orthogonal to the z axis. Interproton vectors that make an angle close to the "magic angle" of 54.7° with the z axis have vanishingly small dipolar couplings.

The HNHA experiment yields only the magnitude of the coupling and not its sign. So, in the absence of a scalar component to the coupling, only the absolute value is available, and a potential energy function must be used that ensures agreement between the structure and the absolute value of the ^1H - ^1H dipolar coupling. Although this dramatically increases the number of local minima in the energy landscape during structure calculation, a substantial set of such couplings measured from a single HNHA 3D spectrum was able to improve the quality of the three-dimensional structure of the protein ubiquitin considerably.⁷⁶ A problem with both this and other quantitative J correlation experiments⁷⁷ is that confusing

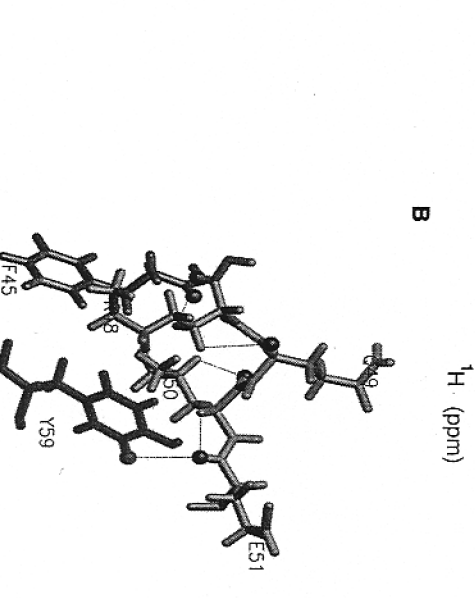
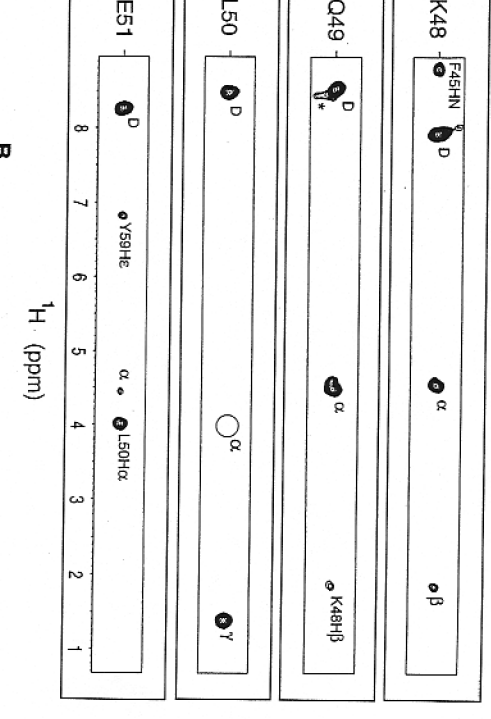


FIG. 9. (A) Strip cross sections taken parallel to the F_2 axis through the 600-MHz 3D HNHA spectrum of ubiquitin, at the (F_1 , F_3) positions of the amides of residues Lys⁴⁸-Glu⁵¹. (B) Corresponding chemical structure of ubiquitin showing interresidue connectivities observed in the HNHA spectrum, including a correlation between Phe⁵⁹-H^e and Glu⁵¹-H^N, are marked by dashed lines. From N. Tjandra and A. Bax, *Science* **278**, 1111 (1997).

artificial peaks can appear if three or more protons have significant couplings to the proton observed during detection. These multispin effects, which can result in three-spin, single quantum coherence during the evolution period, can lead to relatively intense, undesirable peaks that can be difficult to identify.

Tian *et al.* have described an interesting alternative method for deriving ^1H - ^1H couplings, ($J + D$)_{HH}, from the cross-peak to diagonal peak ratio in a

⁶⁹ H. Kessler, M. Gehrke, and C. Griesinger, *Angew. Chem. Int. Ed. Engl.* **27**, 490 (1988).

⁷⁰ T. Prasch, P. Grosche, and S. J. Glaser, *Angew. Chem. Int. Ed. Engl.* **37**, 802 (1998).

⁷¹ F. Lohr, J. M. Schmidt, and H. Ruterjans, *J. Am. Chem. Soc.* **121**, 11821 (1999).

⁷² M. L. Cai, H. Wang, E. T. Olejniczak, R. P. Meadows, A. H. Gunasekera, N. Xu, and S. W. Fesik, *J. Magn. Reson.* **139**, 451 (1999).

⁷³ G. Oetting, M. Ruckert, M. H. Levitt, and A. Moshtref, *J. Biomol. NMR* **16**, 343 (2000).

⁷⁴ W. Peti and C. Griesinger, *J. Am. Chem. Soc.* **122**, 3975 (2000).

⁷⁵ G. W. Vuister and A. Bax, *J. Am. Chem. Soc.* **115**, 7772 (1993).

⁷⁶ N. Tjandra, J. Marquardt, and G. M. Clore, *J. Magn. Reson.* **142**, 393 (2000).

⁷⁷ S. Grzesiek, H. Kuboniwa, A. P. Hinck, and A. Bax, *J. Am. Chem. Soc.* **117**, 5312 (1995).

CT-COSY experiment.⁷⁸ The method was demonstrated for a carbohydrate in a bicelle solution and requires a resolvable diagonal resonance. Although in proteins this requirement would preclude measurement of the majority of ^1H - ^1H couplings, the measurement can be extended to 3D, where ^{15}N is the third dimension, making it more widely applicable.⁷⁹ Alternatively, even the qualitative information regarding the size of a cross peak in a regular COSY spectrum can present useful information on the approximate value of the ^1H - ^1H coupling. One hundred such couplings, measured for the palindromic Dickerson dodecamer, were found to be quite useful for refining the structure of this DNA fragment.⁸⁰ Refinements to this approach may make ^1H - ^1H coupling measurement considerably more quantitative, and thereby even more useful.¹⁴

4. Alignment Media for Macromolecules

As mentioned earlier, a prerequisite for studying macromolecules in a liquid crystalline phase is that the order imposed on the macromolecule be very small, typically less than 0.002. The order of the liquid crystal particles themselves is invariably much higher, in the 0.5–0.85 range. Clearly, in order to have such a weak alignment for the solute in the strongly oriented liquid crystalline medium, interaction between the macromolecule and the liquid crystal must be very weak. The medium must also be aqueous, such that the proteins or nucleic acids remain in their natural environment. An efficient way to satisfy these conditions is the use of a very dilute ($\leq 10\%$ w/v) lyotropic nematic liquid crystalline medium, where the nematogenic unit itself is a large particle. In a liquid crystalline phase, the weak steric and electrostatic interaction between liquid crystal particles causes their cooperative alignment. There is a lower limit for the nematogen concentration, c_n , required to form a stable liquid crystalline phase. If the sample is diluted below this threshold, it separates into an isotropic phase with concentration c_i and a nematic phase, with the c_n being 5–20% higher than c_i . The aspect ratio of the nematogenic particle is a critical determinant for the lowest concentration at which they adopt a liquid crystalline phase. The time needed for formation of a homogeneous liquid crystalline phase strongly depends on the nematogen concentration and can be very long for concentrated samples, but also for samples that are close to the threshold concentration, where separation between microscopic aligned and isotropic domains takes place.

4.1. Bicelles

Bicelles were the first liquid crystalline medium used for weak alignment of proteins and DNA.^{33,35} These are planar micelle particles usually consisting of regular saturated phospholipids. Most commonly, a mixture of dimyristoylphosphatidylcholine (DMPC) and dihexanoylphosphatidylcholine (DHPC) is used. DMPC makes up the bilayer, which constitutes the plane of the micelle, and the DHPC detergent mostly covers the rim. Bicellar liquid crystals were originally developed by Prestegard, Sanders and co-workers for the purpose of

Much liquid crystal work has focused on a phase consisting of the cesium salt of perfluoro-octanoic acid.⁸¹ These molecules assemble into oblate spheroidal particles with semiaxes of approximately 11 and 40 Å. Because of the relatively small aspect ratio, the lowest concentration at which these disks adopt a nematic liquid crystalline phase is rather high, ca 12%. At this high a concentration, nematic particles are spaced by less than 100 Å. Therefore, in such a medium solute macromolecules would be confined much too strongly, resulting in a degree of order that is much larger than 0.002. The degree of macromolecular order is also increased by the high surface charge of the perfluoro-octanoate particles. The resulting strong degree of alignment gives rise to large dipolar ^1H - ^1H couplings, and vanishingly weak, unresolvable ^1H multiplets.

All liquid crystalline media that have turned out to be successful for weak ordering of proteins and nucleic acids consist of much larger (> 500 Å), water-soluble particles, with relatively low surface charge densities ($\leq 0.5 \text{ e nm}^{-2}$). They all show a high macroscopic viscosity as a result of interaction between the liquid crystal particles. However, rotational diffusion of the macromolecule itself is virtually unchanged relative to that in pure water, and relaxation rates are not measurably affected by the liquid crystal, unless it has a weak affinity to bind to the liquid crystal particle. In the latter case, the degree of order typically is much too large anyway, so this case is of little practical interest. For all lyotropic liquid crystals discussed below, the degree of order imposed on the solute can be adjusted by changing the concentration of the liquid crystal itself over the range where it yields an ordered phase. There is not yet a single, ideal liquid crystal. For example, phospholipases without inhibitors cannot be studied in bicelles as they break down the phospholipids, active proteases can destroy phage-based liquid crystals, other proteins may stick to phospholipids, or the surface charge distribution of the liquid crystal may cause too strong an electrostatic interaction with the solute. Also, liquid crystals require some degree of surface charge to keep their order and may fail to remain liquid crystalline at high salt concentrations. Below, several of the most widely used systems are briefly discussed.

⁷⁸ F. Tian, P. J. Bolon, and J. H. Prestegard, *J. Am. Chem. Soc.* **121**, 7712 (1999).

⁷⁹ F. Tian, C. A. Fowler, E. R. Zartler, F. A. Jenney, M. W. Adams, and J. H. Prestegard, *J. Biomol. NMR* **18**, 23 (2000).

⁸⁰ N. Tjandra, S. Tate, A. Ono, M. Kainosho, and A. Bax, *J. Am. Chem. Soc.* **122**, 6190 (2000).

studying lipophilic molecules, anchored in these highly ordered membranes.^{82,83} The DMPC/DHPC combination was found to be particularly robust. When the temperature rises above 25°, the system switches from isotropic to a nematic liquid crystalline phase.³² This temperature corresponds to the melting temperature of DMPC, i.e., the temperature at which the saturated alkane chains of DMPC melt from a crystalline or gel state, in which the alkane chains are all trans, to a flexible, liquid crystalline phase. Above this transition temperature the sample has high macroscopic viscosity and tends to be very slightly opaque. However, as discussed below, whether the medium will form a homogeneous nematic liquid crystalline phase or not depends on a number of other factors as well. Below 25° the solution remains clear and unordered, and no details on the shape or size distribution of such micelles have yet been reported.

The phase diagram of the DMPC/DHPC mixture is very complex and depends on a large number of variables, including the absolute concentration, the molar ratio [DMPC]/[DHPC] = q , temperature, ionic strength, and on the presence of charged amphiphilic molecules such as sodium dodecyl sulfate (SDS) or cetyl trimethylammonium bromide (CTAB).

A simple model has been proposed for the bicelles in which the detergent and long chain lipids are strictly partitioned in the rim and planar face of the bicelle.⁸⁴ As the surface of the planar face of the bicelle increases with the square of its radius, R , its circumference increases linearly with R . Consequently, assuming that the surface ratio of the planes over the rim equals q , R can be derived from:

$$q = 2\pi R^2 / [2\pi r(\pi R + 2r)] \quad (9)$$

where $2r$ is the thickness of the bilayer.⁸⁴ Clearly, the assumption of strict partitioning of the two types of phospholipids is an oversimplification, and this will influence the size of the bicelle. For dilute bicelle solutions, another important factor is the concentration of free detergent, which is in dynamic equilibrium with bicelle-bound detergent. For DHPC, the concentration of free detergent in equilibrium with bicelle bound DHPC is temperature dependent and increases from ca 3 mM at 20° to ca 5 mM at 37°.⁸⁵ The same free DHPC concentration in the liquid crystalline phase was also found by two different approaches.^{36,86} The presence of free DHPC increases the effective q ratio, and thereby the size of the bicelles. Therefore, in dilute bicelle media, an effective ratio,

$$q_{\text{eff}} = [\text{DMPC}] / [\{\text{DHPC}\} - \{\text{DHPC}_{\text{free}}\}] \quad (10)$$

must be used when employing Eq. (9) for estimating bicelle size.

When going to more dilute bicelle solutions, the DMPC/DHPC ratio becomes increasingly critical. Too low a ratio results in disks that are too small to align cooperatively at the low concentration used. Too high a ratio can result in nonplanar bicelles that may collapse to form spherical particles with holes, where the solvent exposed rim of the hole is covered by DHPC. Clearly, planarity of the bicelle is essential to formation of the liquid crystalline phase, and it appears that $q_{\text{eff}} \approx 5$ is about the upper limit at which stable planar bicelles can be obtained. With $2r \approx 40$ Å, this corresponds to a bicelle diameter of 650 Å.

Intrinsically, DMPC/DHPC bicelles can form a liquid crystalline phase over the temperature range of 25–45°. However, near the lower end of this range (25–30°), dilute samples (<70 mg/ml) tend to be unstable and they frequently separate into an aligned and an isotropic phase. This can be prevented by addition of a small molar fraction (typically 1–3%, relative to [DMPC]) of charged amphiphiles, such as the CTAB (positive), or SDS (negative).⁸⁷ Alternatively, charged phospholipids such as DMP-serine (negative) or dimyristoyltrimethylammonium propane (positive) can be used. Charging the bicelles in this manner helps prevent phase separation and widens the part of the phase diagram over which the liquid crystalline phase is stable. However, it also will result in an electrostatic potential that repels and attracts oppositely charged groups of the solute, and generally causes a change in both the orientation and magnitude of the alignment tensor. This can be a highly beneficial side effect, as it permits measurement of dipolar couplings under multiple orientations of the protein.⁸⁸ However, frequently this change in orientation is not very large, so that if more than two different samples are prepared in this manner, they simply yield alignment tensors that are simple linear combinations of each other.⁸⁹

Preparation of bicelle samples is straightforward and has been described in detail elsewhere.⁸⁵ Typically, we obtain best results using dry powder DHPC and DMPC as starting material, and add the required amount of buffer to the detergent, prior to adding this to DMPC. Because of the hygroscopic nature of DHPC, it is recommended to work in a dry box for accurately determining the quantity of detergent being used. It is also important to ensure that the buffer contains a sufficiently high concentration (≥ 1 mM) of an antibacterial agent such as sodium azide. Dissolving the DMPC in the buffer/detergent mixture can be accelerated by repeated vortexing, heating and cooling cycles, but in practice we find it easier to simply leave the sample at or slightly below room temperature for a few days, which always results in a clear solution.

4.1.1. Other Bicelle Mixtures. Regular phospholipids are subject to acid- and base-catalyzed hydrolysis of the carboxyester linkage between the alkyl chain and

⁸² C. R. Sanders and J. H. Prestegard, *Biophys. J.* **58**, 447 (1990).

⁸³ C. R. Sanders and J. H. Prestegard, *J. Am. Chem. Soc.* **113**, 1987 (1991).

⁸⁴ R. R. Vold and R. S. Prosser, *J. Magn. Reson. Ser. B* **113**, 267 (1996).

⁸⁵ M. Ottiger and A. Bax, *J. Biomol. NMR* **12**, 361 (1998).

⁸⁶ B. E. Ramirez, O. N. Voloshin, R. D. Camerini-Otero, and A. Bax, *Prot. Sci.* **9**, 2161 (2000).

⁸⁷ J. A. Losonczi and J. H. Prestegard, *J. Biomol. NMR* **12**, 447 (1998).

⁸⁸ B. E. Ramirez and A. Bax, *J. Am. Chem. Soc.* **120**, 9106 (1998).

⁸⁹ J. Sass, F. Corder, A. Hoffmann, A. Cousin, J. G. Omicinski, H. Lowen, and S. Garzesek, *J. Am. Chem. Soc.* **121**, 2047 (1999).

the glycerol backbone. The rate of hydrolysis is minimal at pH 6.5, but rapidly increases once the pH differs by more than one unit from this value.⁸⁵ Use of ether lipids, where the carboxyester bond is replaced by an ether linker, can prevent this hydrolysis, and such samples can be stable over a very wide range of pH^{90,91} for periods of several years.

As most of the hydrolysis appears to take place on the water-soluble DHPG detergent, and to a much lesser extent on the long-chain phospholipid, a cheaper solution is the use of a nonhydrolyzable detergent such as CHAPS or CHAPSO.^{92,93} Use of a different detergent may sometimes also improve the stability of the protein/liquid crystal solution. For example, in some cases, the protein binds one type of detergent, but not the other, and use of the nonbinding detergent is clearly preferable. The binding of detergent is most easily monitored by addition of 5 mM detergent to a protein sample, and comparison of the HSQC spectrum with that of the free protein. A drawback with detergents other than DHPG is that the bicelle phase diagram has not yet been explored as widely, and some trial-and-error adjustment may be necessary to find optimal conditions.

The temperature range over which the bicelles are liquid crystalline can be adjusted either by introducing a small fraction of monounsaturated DMPC, which lowers the melting temperature of the alkane chain,⁸⁵ or by using shorter alkane chains. Use of shorter alkane chain phospholipids, such as dilauoyl-PC (12-C chains)⁹³ or ditridodecanoyl-PC (13 carbons),⁹⁰ lowers the transition temperature by about 12° and 6°, respectively, and increases the upper temperature limit as well. However, the macroscopic viscosity of these liquid solutions below the transition temperature tends to be much higher than for DMPC/DHPC bicelles, such that preparation of the sample can be more cumbersome, particularly when using a microcell.

4.2. Filamentous Phage

Use of a liquid crystalline solution consisting of filamentous phages for aligning macromolecules was introduced simultaneously and independently by Clore *et al.* and by Pardi and co-workers.^{94–96} Clore *et al.* used a medium consisting of the filamentous phage *fd*, and also demonstrated the potential of tobacco mosaic virus (TMV). The Pardi group used the phage *PfI*, which is similar to *fd*, but which at

a contour length of ca 2 μm is nearly twice as long. Both phages have a diameter of 6.5 nm, and a persistence length of ca 2 μm . As a result of the very high aspect ratios of these particles, solutions can remain liquid crystalline down to very low concentrations, as low as a few mg/ml. Although it was suggested that liquid crystallinity is independent of ionic strength, we find this to be true only at the higher phage concentrations (M. Zweckstetter, unpublished), whereas at lower concentrations (<13 mg/ml for *PfI*) the degree of alignment becomes sensitive to ionic strength, and at very high salt concentrations the samples become isotropic. The negative surface charge (ca 0.5 e per nm^2) is necessary to maintain a uniform suspension of these large particles. When the pH is below 6, partial protonation of the glutamate and aspartyl sidechains of the phage coat protein reduces the net charge of the virus particle and the sample loses its liquid crystallinity.

As highlighted by Clore *et al.* for an immunoglobulin-binding domain of streptococcal protein G, the alignment tensor in the phage medium can be very different from that in the bicelle medium.⁹⁴ This is strongly advantageous as it permits measurement of dipolar couplings relative to two independent axis systems, thereby resolving much of the degeneracy that occurs in interpreting a dipolar coupling in terms of two orientational variables, θ and ϕ in Eq. (3e) (see also Section 5.3). The phage particles are aligned with their long axis parallel to the magnetic field. Therefore, if the alignment of solute macromolecules were caused exclusively by steric interaction, the alignment tensor would be very similar to that in the bicelle medium. In practice, the alignment tensors in phage and bicelle media tend to be quite different as there also are relatively strong electrostatic interactions between the phage and the solute (see also Section 5.3).

The phage-based liquid crystal medium is particularly easy to use. *PfI* phage can be obtained commercially (Asla Labs, <http://130.237.129.141//aslaphage.htm>), or can be prepared in-house with relatively little effort.⁹⁷ Another important advantage relative to the bicelle medium is that it is easy to recover the protein from the phage medium. Centrifugation is typically sufficient to remove the phage, which precipitates to form a pellet, whereas the protein remains in the supernatant. The phage pellet can be resolubilized and recycled for making a new liquid crystalline medium. In contrast to the bicelle medium, however, the phage-containing solution cannot be stored in a freezer, and clearly it cannot be lyophilized.

4.3. Cetylpyridinium-Based Media

Ternary mixtures of cetylpyridinium chloride (CPCl) or bromide (CPBr), hexanol, and NaCl or NaBr in water can form stable liquid crystalline phases over a wide range of conditions. Prosser *et al.*⁹⁸ demonstrated that the CPCl version

⁹⁰ M. Ottinger and A. Bax, *J. Biomol. NMR* **13**, 187 (1999).
⁹¹ S. Cavagnetto, H. J. Dyson, and P. E. Wright, *J. Biomol. NMR* **13**, 387 (1999).
⁹² C. R. Sanders and G. C. Landis, *Biochemistry* **34**, 4030 (1995).
⁹³ H. Wang, M. Ebertstadt, E. T. Olejniczak, R. P. Meadows, and S. W. Fesik, *J. Biomol. NMR* **12**, 443 (1998).

⁹⁴ G. M. Clore, M. R. Starich, and A. M. Gronenborn, *J. Am. Chem. Soc.* **120**, 10571 (1998).
⁹⁵ M. R. Hansen, M. Rance, and A. Pardi, *J. Am. Chem. Soc.* **120**, 11210 (1998).

⁹⁶ M. R. Hansen, L. Mueller, and A. Pardi, *Nat. Struct. Biol.* **5**, 1065 (1998).
⁹⁷ M. R. Hansen, P. Hanson, and A. Pardi, *RNA-Ligand Interact. A* **317**, 220 (2000).
⁹⁸ R. S. Prosser, J. A. Losonczi, and I. V. Shlyanovskaya, *J. Am. Chem. Soc.* **120**, 11010 (1998).

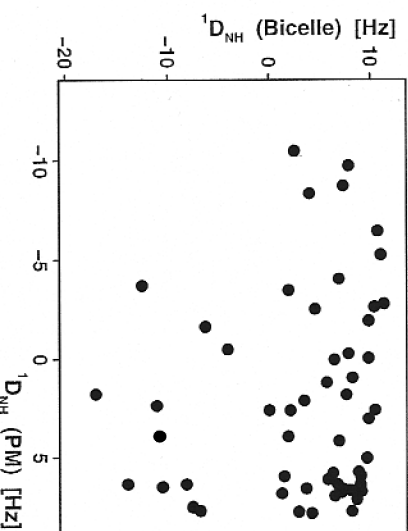


FIG. 10. Plot of ${}^1D_{\text{NH}}$ couplings measured for ubiquitin backbone amides in nearly neutral bicelles (50 mg/ml) vs values measured in a 1 mg/ml PM medium.

yielded alignment for the protein ubiquitin, and Barrientos *et al.*⁹⁹ described the use of the CPBr-based medium. Remarkable differences were found between the CPBr- and CPCl-based liquid crystals, with CPBr being more suitable for low ionic strength measurements (25–40 mM NaBr) and the CPCl system requiring higher salt concentrations (200–500 mM NaCl).⁹⁹

The CPBr system has been characterized in more detail than the CPCl medium, and the media appear to be optimally suited for protein alignment when using a 1:1.33 (w/w) ratio of CPBr:hexanol. The ${}^2\text{H}$ solvent quadrupolar splitting increases approximately linearly from 5 to 20 Hz when the concentration is increased from 30 to 65 mg/ml. Alignment of a small 56-residue protein domain in this medium yielded a degree of protein alignment comparable to what was observed in 28 mg/ml *fd*, or 50 mg/ml bicelle media. The alignment tensor was found to be more similar (but opposite in sign) compared to phage than relative to that in the bicelle medium. Very few data on proteins are available to date for the CPBr and CPCl systems, and it remains to be investigated how widely applicable they are. Considering that CPBr is a surfactant, problems for some systems that interact with this surfactant may be anticipated, analogous to problems encountered with proteins that interact with DMPC or DHPC in bicelle media. Also, surface charge density is rather high.

In contrast to the phage media, the CPBr and CPCl media are positively charged. Therefore, it may be anticipated that phage and CPBr or CPCl media will complement one another; if a protein is strongly positively charged it is expected to bind weakly to phage, but not to cetylpyridinium, and vice versa.

The morphology of the CPBr and CPCl media has not been established with certainty yet. It may be either a lamellar phase or the so-called Helfrich type,¹⁰⁰ or it may consist of cylindrical, wormlike elongated micelles.⁹⁹

4.4. Purple Membrane Fragments

Bacteriorhodopsin is an integral membrane protein with seven transmembrane helices. It is present at extremely high density (75% w/w) in the cell membrane of *Halobacterium salinarium*.¹⁰¹ Fragments of this so-called purple membrane (PM) are easily prepared in large quantities and have been used for a wide array of optical and biophysical experiments. The PM fragments have an average diameter of about 1 μm , and this is sufficiently large that the total magnetic susceptibility anisotropy of such a particle causes it to align nearly 100% when placed in a strong magnetic field (≥ 11 T), with the membrane plane orthogonal to the direction of

the magnetic field.¹⁰² So, in contrast to the bicelle, phage, and CPBr systems, PM does not need to form a liquid crystalline phase for obtaining alignment.

The strong net negative surface charge of PM causes very weak transient binding of solute proteins that carry clusters of positively charged groups on their surfaces, and thereby can result in net alignment.^{88,103} The electrostatic interactions are typically weak enough not to distort the structure of globular proteins. However, as is the case with all liquid crystal studies in this chapter, when studying flexible regions in a protein, care must be taken when interpreting the dipolar coupling data as the protein only transiently interacts with the liquid crystal. Interaction with the nematogen may be favored when the flexible region temporarily adopts a given shape, whereas other, nonbinding conformations of the flexible region may not be sampled.

The fact that the PM surface orients orthogonal to the magnetic field causes the induced alignment tensor to be twofold larger compared to vertical surfaces, such as found in bicelle and phage media. Therefore, frequently only very small quantities of PM are needed to cause significant alignment. For example, alignment of ubiquitin in a 1 mg/ml PM suspension yields dipolar couplings that are comparable in magnitude to what is obtained in a 50 mg/ml bicelle medium (Fig. 10).

¹⁰² B. A. Lewis, C. Rosenblatt, R. G. Griffin, J. Courtemanche, and J. Herzfeld, *Biophys. J.* **47**, 143 (1985).

⁹⁹ L. G. Barrientos, C. Dolan, and A. M. Gronenborn, *J. Biomol. NMR* **16**, 329 (2000).

¹⁰⁰ K. M. McGrath, *Langmuir* **13**, 1987 (1997).

¹⁰¹ D. Oesterhelt and W. Stoeckenius, *Methods Enzymol.* **31**, 667 (1974).

As expected, alignment of proteins in a PM suspension strongly decreases with increasing ionic strength. However, the PM medium itself is also affected by increases in salt concentration. At low ionic strength ($\leq 10 \text{ mM NaCl}$), the suspension remains homogeneous and easily aligns in the magnetic field. However, if the ionic strength is increased to 50 mM , a 10 mg/ml PM suspension starts aggregating and, after 24 hr, it no longer aligns in the magnetic field. Interestingly, the alignment persists indefinitely, even if the sample is later removed, stored in a refrigerator, and subsequently reinserted in the magnetic field. Presumably, at higher ionic strength, electrostatic repulsion between the PM fragments is decreased and the edge of one PM fragment can fuse with another fragment. If the fragments are aligned when fusing occurs, it can only happen in an "edge-to-edge" manner, whereas for unoriented samples the edge of one fragment may fuse to the center of another fragment, a process often referred to as clumping. Sass *et al.* have demonstrated that PM fragments can be stabilized by an acrylamide gel, even at high ionic strength.¹⁰⁴ If gelling occurs while the PM fragments are aligned, this stabilizes such fragments presumably indefinitely.

As can be seen in Fig. 10, the dipolar couplings observed in the PM medium are very different from those observed in the bicelle medium and therefore contain unique information. As discussed by Sass *et al.*, the alignment introduced by PM results from the sum of the electrostatic component and a steric component, but the electrostatic component is by far larger.⁸⁹

4.5. Cellulose Crystallites

Yet another liquid crystal medium suitable for macromolecule alignment has been proposed.¹⁰⁵ It consists of cellulose crystallites that have been prepared by careful sulfuric acid hydrolysis of natural cellulose fibers, derived either from wood pulp or from filter paper. In various steps, a subset of the crystallites is isolated that has a relatively uniform size distribution, with lengths of several hundred nanometers and cross sections that are 20–40 times smaller. The crystallites carry sulfate groups and are therefore negatively charged, but carry considerably less surface charge than filamentous bacteriophages and therefore yield less electrostatic and more steric solute alignment. The long axis of the cellulose crystallites is orthogonal to the field, which will result in twofold weaker alignment than would be obtained with crystallites parallel to the magnetic field.

The example shown by Fleming *et al.*¹⁰⁵ is for a 20 kDa protein, dissolved in a 80 mg/ml suspension of crystallites in water containing 20 mM sodium acetate. Because of the lower surface charge of these cellulose particles compared to phage,

it is expected that the medium will be sensitive to ionic strength, i.e., that the minimum concentration needed for obtaining a nematic liquid crystalline phase will increase rapidly with increasing ionic strength.¹⁰⁶

4.6. Alkyl Poly(ethylene glycol) Based media

Another potentially very interesting liquid crystal medium for protein and nucleic acid alignment has been introduced by Rückert and Otting.¹⁰⁷ It is a lyotropic liquid crystal consisting of a mixture of alkyl poly(ethylene glycol) and hexanol. One advantage of this system is that alkyl poly(ethylene glycol) type compounds generally do not tend to bind to proteins. Also, Rückert and Otting note that the surface of the liquid crystal, which is indicated to have a lamellar phase, is non-charged, and therefore is expected to yield predominately steric alignment. Also, the liquid crystal is stable indefinitely (provided the concentration of hexanol does not decrease as a result of slow evaporation) and is applicable over a wide pH range and a considerable temperature range of $10\text{--}40^\circ$, which is tunable by varying the type of alkyl poly(ethylene glycol).

The different alkyl poly(ethylene glycol) compounds are referred to as C_mE_n , where m is the number of carbons in the alkyl group, and n is the number of ethylene glycol units. Working with the recommended hexanol to C₁₂E₅ molar ratio of 0.96 (5 w% C₁₂E in H₂O) yields a particularly stable liquid crystal that is easy to prepare. C₁₂E₅ is commercially available (Sigma-Aldrich, St. Louis, MO). In many cases, the sample can simply be recovered from the liquid crystal by extensive dialysis.

The medium has been demonstrated for measurement of dipolar couplings in the protein BPTI, a double-stranded DNA fragment, and a complex between the protein ArgR-N and its operator DNA, indicating wide applicability of the system.

4.7. Polyacrylamide Gel

In order to prevent sedimentation, suspension of large particles such as phages, bicelles, and cellulose requires a repelling interaction. The required net surface charge frequently causes stronger protein alignment, and sometimes it becomes too strong for convenient measurement. For example, the protein ubiquitin in a filamentous phage medium can only be studied at high salt concentrations. Other proteins can cause the liquid crystal particles to aggregate and precipitate. Tycko *et al.* have proposed the use of a different type of medium for aligning proteins; the use of a compressed gel.¹⁰⁸ This gel is highly (>90%) hydrated but is relatively stiff because of the presence of extensively cross-linked polyacrylamide.

¹⁰⁶ X. M. Dong, T. Kimura, J. F. Revol, and D. G. Gray, *Langmuir* **12**, 2076 (1996).

¹⁰⁴ H. J. Sass, G. Musco, S. J. Stahl, P. T. Wingfield, and S. Grzesiek, *J. Biomol. NMR* **18**, 303 (2000).

¹⁰⁵ K. Fleming, D. Gray, S. Prasannan, and S. Matthews, *J. Am. Chem. Soc.* **122**, 5224 (2000).

¹⁰⁷ M. Rückert and G. Otting, *J. Am. Chem. Soc.* **122**, 7793 (2000).

¹⁰⁸ R. Tycko, F. J. Blanco, and Y. Ishii, *J. Am. Chem. Soc.* **122**, 9340 (2000).

Protein can be soaked into the gel, and when the gel is compressed, pore shape inside the gel becomes nonrandom with respect to the direction in which the pressure is applied.

In the implementation by Tycko *et al.*,³ 3-mm OD cylindrically shaped gels are prepared, which are inserted in a regular 5-mm NMR tube. Application of pressure by means of a plunger to the top of the gel, until its diameter matches the inside diameter of the NMR tube, causes the deformation of the gel pores and thereby generates the solute alignment.

The potential advantages of this system are that it is very inert, carries virtually no charge, and can be done over a wide range of polymer density, temperature, pH, and ionic strength. Also, it generally will be relatively easy to extract the solute from the gel. Potential disadvantages may be that it can be difficult to make the system sufficiently homogeneous for obtaining very high resolution spectra, and it is not yet known how homogeneous the dipolar coupling will be across the sample, i.e., whether diffusion between pores in the gel is sufficiently fast to average out the different degrees of alignment associated with the different locations.

An alternate method for gel preparation was proposed by Grzesiek and co-workers.¹⁰⁴ In their method, a 10-mm cylindrical gel is dried, upon which it shrinks considerably, allowing its insertion into a 5-mm NMR tube. Rehydration, with the protein containing solution yields the aligned medium, with the macromolecules diffused into the gel. In contrast to Tycko's method, here the director of alignment is orthogonal to the magnetic field because this is the direction in which the gel is compressed. Intrinsically, the order obtained with Grzesiek's approach is therefore twofold lower, but the higher attainable compaction compensates for this. Practical issues appear to be concerned primarily how homogeneous the gel can be made. If not perfectly homogeneous, there will be a heterogeneous distribution of stronger and weaker aligned regions, causing some line broadening, in particular for ¹⁵N-¹H and ¹³C-¹H sites with large dipolar interactions. Also, the presence of the gel has an adverse effect on the rotational diffusion rate of the protein, causing some (15–50%) line broadening.¹⁰⁴

As Tycko *et al.* point out, the use of polyacrylamide gels offers the tantalizing possibility to induce biaxial alignment, by using different degrees of gel compression in the x, y, and z directions. Such a sample could then subsequently be reoriented relative to the magnetic field, analogous to single-crystal solid-state NMR.¹⁰⁸ If sufficient biaxiality can be induced, this potentially could dramatically simplify structure determination by NMR and yield extremely high resolution structures.

5. Relation between Alignment and Shape

Tjandra *et al.* demonstrated that in a bicelle medium the principal axes of the molecular alignment tensor closely coincide with those of the rotational diffusion tensor.^{33,109} This shows that in this nearly neutral medium, alignment is defined

by the solute's shape. The alignment tensor can be modified by adding a net charge to the bicelles, by doping them with either CTAB (+) or SDS (−). This demonstrates that electrostatic interactions can also play a role. In fact, for an oriented medium of strongly negatively charged, rod-shaped viral particles, or oriented purple membrane fragments, electrostatic interactions often dominate alignment of solute proteins.

A simple steric model has been proposed that quantitatively describes the relation between the solute's shape and its alignment in lyotropic liquid crystals.¹¹⁰ So far, it has only been demonstrated for the case of (nearly) neutral particles, such as bicelles, but preliminary results indicate that the method can easily be extended to account for the effect of charge.

In the so-called steric-obstruction model, the solute sample can be simulated as a collection of randomly oriented, uniformly distributed molecules, from which the fraction that sterically clashes with the ordered array of liquid crystal particles is removed. For example, for a disk-shaped nematogen and a rod-shaped solute molecule, a larger fraction of molecules oriented orthogonal to the disks will be obstructed than of molecules parallel to the disk surface, resulting in net ordering of the remaining, nonobstructed molecules. For each nonobstructed molecule a Saupe order matrix is calculated, using Eq. (2). Averaging of the Saupe matrices for all nonobstructed proteins than yields the sterically predicted alignment tensor.¹¹⁰ In an extension of this method that accounts also for the effect of electrostatics, different weighting factors are given to each of the nonobstructed solute molecules, depending on the Boltzmann factor calculated when taking the electrostatic potential into account (M. Zweckstetter, unpublished results).

Figure 11 shows the correlation between the ¹⁵N-¹H dipolar couplings measured for the Ig binding domain of streptococcal protein G, and that predicted from its 1.0 Å crystal structure, using an alignment tensor that is not best-fitted to the data, but calculated on the basis of its shape.¹¹¹ When electrostatics is ignored, the predicted alignment tensors for bicelle and phage media are very similar. However, the experimentally observed dipolar couplings in the two media are very different and, as expected, good agreement is only observed for the bicelle medium (Fig. 11). When electrostatic terms are included in the calculations for the phage medium, the agreement becomes nearly as good as for the neutral bicelle medium (M. Zweckstetter, unpublished results).

The ability to predict the alignment tensor on the basis of the molecule's shape has several interesting applications. First, it can be used to validate a structure determined by NMR or crystallography. For example, it is possible to distinguish between different oligomeric states, which can sometimes be difficult to identify by conventional NMR. Second, it permits selection of different relative orientations of the two halves in a homodimer. For example, work by Bewley and Clore indicates

¹¹⁰ M. Zweckstetter and A. Bax, *J. Am. Chem. Soc.* **122**, 3791 (2000).

¹¹¹ J. P. Derrick and D. B. Wigley, *J. Mol. Biol.* **243**, 906 (1994).

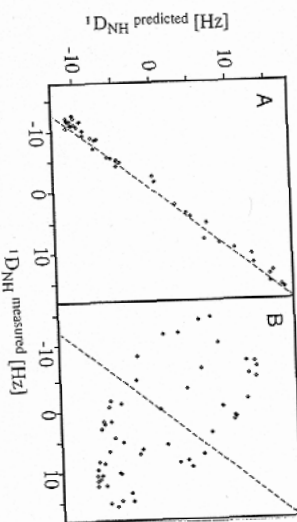


FIG. 11. Correlation between experimental $^1D_{NH}$ values and couplings calculated from the shape predicted alignment tensor for the Ig-binding domain of streptococcal protein G. (A) Dipolar couplings measured in 50 mg/ml bicelle medium and (B) measured in 28 mg/ml *fd*. [Adapted from Zweckstetter and Bax, *J. Am. Chem. Soc.* **122**, 3791 (2000).]

that in solution the average relative orientation of the two halves of the domain-swapped homodimeric form of cyanovirin-N is quite different from that seen in its X-ray structure.¹¹² Third, ongoing work indicates that the relation between shape and alignment can yield quantitative information on interdomain flexibility in multidomain systems.

The program for calculating the alignment tensor can be downloaded from <http://spin.niddk.nih.gov/bax>.

6. Use of Multiple Alignment Media

As mentioned above, solute alignment is defined by both steric and electrostatic interaction. So, by using nearly neutral liquid crystals, such as bicelles or the alkyl poly(ethylene glycol) medium, and a charged medium such as phage or the cetylpyridinium-based phase, a single molecule can be studied using two or more independent alignment tensors. As illustrated in Fig. 12, this removes much of the degeneracy in the relation between dipolar coupling and internuclear vector orientation.⁸⁸ A dipolar coupling measured in a given medium defines the internuclear vector to be on one of two oppositely oriented cones. The alignment tensor in a second medium will generally be oriented differently relative to the molecular frame and a dipolar coupling defines the same vector to be situated on two different cones. The true internuclear vector orientation then must be located on one of the intersections between the two sets of cones (Fig. 12). In the general case of a nonaxially symmetric (rhombic) alignment tensor there are up to eight intersections. If a third, independent alignment tensor can be obtained, this degeneracy may be reduced to twofold. The true orientation and its inverse can never be distinguished from measurements on a single dipolar interaction, and twofold degeneracy is therefore the best that can be achieved for a single vector.

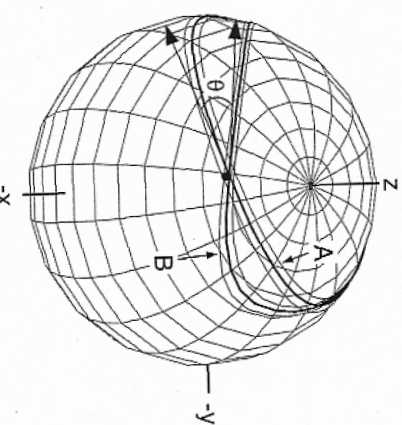


FIG. 12. Orientations of the Gln⁴⁰ N-H vector in ubiquitin compatible with the measured dipolar couplings in undoped bicelles (band A) and in bicelles positively charged by adding CTAB (band B). Orientations are presented in the coordinate frame of the X-ray crystal structure of the protein.¹⁴² The heavy lines correspond to the measured dipolar couplings; thinner lines correspond to orientations when D_{NH} is increased or decreased by 1 Hz. The angle θ at which the two distorted cones intersect equals 29°. The solid dot marks the orientation of the N-H vector in the crystal structure, with hydrogen atom positions model built with the X-PLOR program. (From B. E. Ramirez and A. Bax, *J. Am. Chem. Soc.* **120**, 9106 (1998).)

Besides changing the liquid crystal medium, the alignment tensor may also be altered by subtly changing the protein. For example, when the solution pH is altered such that the surface charge distribution becomes different, this will affect the alignment tensor in charged liquid crystal media. Similarly, if protein preparations are available with and without a His-tag tail, their alignment tensors will generally be different, although not necessarily by a large amount. Also, for a protein with a His-tag, a relatively small change in pH from 6 to 7.5 can significantly alter the alignment tensor. Alternatively, a protein may be studied in the absence and presence of a binding partner, either a natural ligand, an interacting protein, or a covalently linked domain. In the latter case, interpretation of chemical shift changes between the various forms is needed to exclude large-scale rearrangements.

If one-bond dipolar couplings are measured for a set of noncollinear interactions in a chiral fragment of known secondary structure, such as an α helix, there are only four different ways to orient the fragment relative to the alignment tensor. When dipolar couplings are measured in a second, independent medium, this degeneracy can be lifted completely, and the orientation is defined uniquely.¹¹³ This lifting of degeneracy is proving to be particularly important when using dipolar

¹¹³ H. M. Al-Hashimi, H. Valafar, M. Terrell, E. R. Zartler, M. K. Eidness, and J. H. Prestegard, *J. Magn. Reson.* **143**, 402 (2000).

couplings to define molecular structure in the absence of NOE distance restraints or other prior information.

7. Structure Validation

One particularly attractive feature of dipolar couplings is that they can be used in a very direct manner to evaluate the accuracy of any given structure. If the structure is very accurate, dipolar couplings will be in excellent agreement with this structure. In order to evaluate the agreement, one first needs to determine the alignment tensor or Saupe matrix. As mentioned earlier, the most effective method for doing this determines the Saupe matrix elements of Eq. (2c) by simple singular value decomposition. There are five independent elements in the Saupe matrix. In the traceless, diagonalized order matrix there are only two variables that correspond to the magnitude and rhombicity of the alignment tensor, whereas the orientation of this tensor is defined by the three Euler angles needed to rotate from the molecular frame to the frame of the diagonalized alignment tensor. Clearly, for effective validation it is necessary that the number of observables (dipolar couplings) is much larger than the number of variables (five) in the fit. If this condition is not met, corrections can be made for the significance of the correlation in terms of F statistics. For proteins, typically the number of observed dipolar couplings is much greater than five, and the goodness of the fit provides a direct measure for the accuracy of the structure.

Figure 13 shows a typical example of the correlation between measured dipolar couplings and those predicted by two structures of the protein ubiquitin (after best fitting the Saupe matrix to the experimental couplings). The first structure (Fig. 13A) was calculated using a very large number of NOE and J coupling derived angular restraints. It yields a Pearson's correlation coefficient, R^P , of 0.95. The second structure (Fig. 13B) was calculated by additionally including 870 dipolar restraints, which represents all measured dipolar couplings, except for the $^{13}\text{C}^e\text{-}^1\text{H}^e$ dipolar couplings being evaluated. The correlation coefficient between these unused $^1\text{D}_{\text{CH}}$ dipolar couplings and values predicted by the alignment tensor equals 0.98.

Both ubiquitin structures result in high correlations between measured and predicted $^1\text{D}_{\text{CH}}$ dipolar couplings. However, the increase in the correlation coefficient R^P from 0.95 to 0.98 may appear to be rather modest. Because the maximum value of R^P equals 1, R^P is not an ideal parameter for describing the quality of the correlation. Also, in order to avoid confusion with the R factor commonly used in crystallography¹¹⁴ and also in NMR,¹¹⁵⁻¹⁸ we prefer a different definition

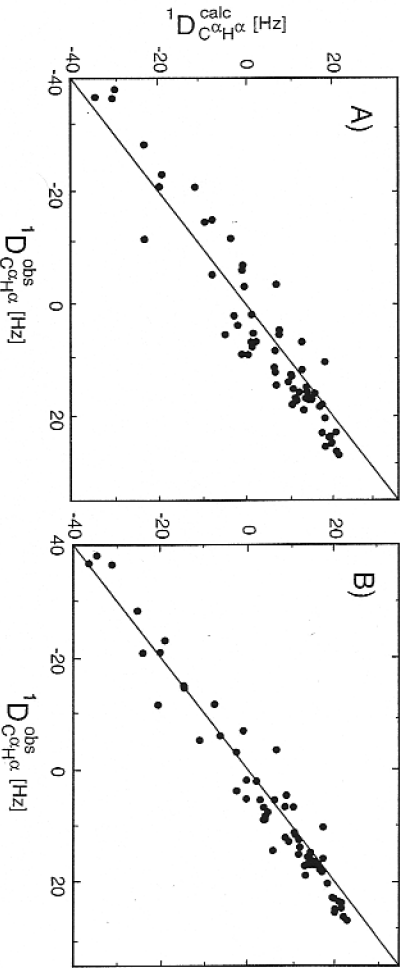


FIG. 13. Plot of experimental ubiquitin $^1\text{D}_{\text{C}\alpha\text{H}}$ couplings vs values calculated after best-fitting the alignment tensor to (A) a structure calculated on the basis of NOEs (>25 per residue, on average) and 90 angular restraints derived from J couplings, and (B) by the additional use of 870 backbone and side-chain dipolar couplings. The correlation coefficient for (A) is 0.954 and for (B) 0.978.

to indicate the goodness of the correlation. To this extent, a quality factor Q is defined^{90,119}:

$$Q = \text{rms}(D^{\text{obs}} - D^{\text{calc}})/\text{rms}(D^{\text{obs}}) \quad (11)$$

where $\text{rms}(D^{\text{obs}} - D^{\text{calc}})$ refers to the root-mean-square of the difference between D^{obs} and D^{calc} values, and $\text{rms}(D^{\text{obs}})$ is a normalization factor. The relation between R^P and Q is shown in Fig. 14. It is important to note that Q is more similar to a "free R factor"^{114,118} as it only should be used when the restraints being evaluated were not included in deriving the structure. If the restraints were included, the value of Q becomes meaningless as it depends primarily on the force constant used in the calculation.

In the above example, $^1\text{D}_{\text{C}\alpha\text{H}}$ dipolar couplings were used and the corresponding Q factor is therefore referred to as $Q^{\text{C}\alpha\text{H}}$. For the two ubiquitin structures discussed above, $Q^{\text{C}\alpha\text{H}}$ equals 0.31 and 0.22. Usually, different types of couplings give comparable Q factors, typically to within ± 0.05 . For the same two ubiquitin structures, Q^{NH} values are 0.27 and 0.18. The Q factor is a rather steep criterion for evaluating quality, and typically it is difficult to obtain protein structures by NMR with Q factors lower than 0.3 when using only NOE restraints. With dipolar restraints included, numbers below 0.2 are attainable, which is comparable to that seen for well-refined crystal structures solved at about 1.5 Å. Note, however, that

¹¹⁴ A. T. Brunger, *Nature* **355**, 472 (1992).

¹¹⁵ P. D. Thomas, V. J. Basus, and T. L. James, *Proc. Natl. Acad. Sci. U.S.A.* **88**, 1237 (1991).

¹¹⁶ C. Gonzalez, J. A. C. Rullmann, A. Bonvin, R. Boelens, and R. Kaptein, *J. Magn. Reson.* **91**, 659 (1991).

¹¹⁷ J. M. Witka, J. Srinivasan, and P. H. Bolton, *J. Magn. Reson.* **98**, 611 (1992).

¹¹⁸ A. T. Brunger, G. M. Clore, A. M. Gronenborn, R. Safranich, and M. Nages, *Science* **261**, 328 (1993).

¹¹⁹ G. Cornilescu, J. L. Marquardt, M. Ottinger, and A. Bax, *J. Am. Chem. Soc.* **120**, 6836 (1998).

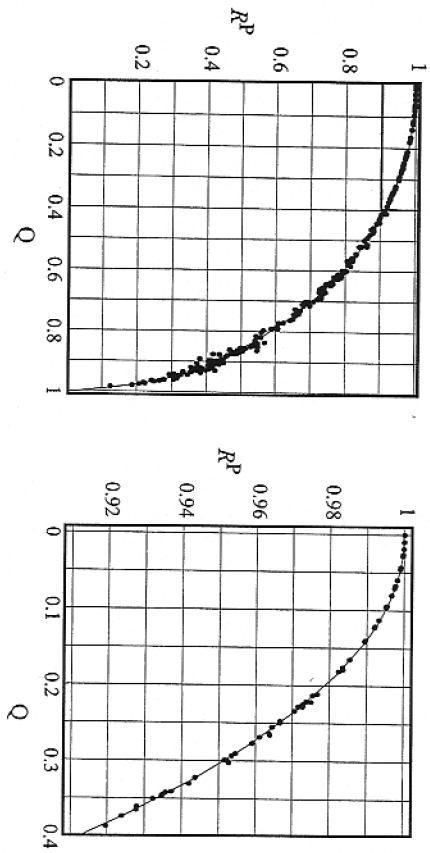


FIG. 14. Relation between Pearson's correlation coefficient, R^P , and Q . [From G. Comilescu and A. Bax, *J. Am. Chem. Soc.* **122**, 2168 (2000).]

Q only evaluates the orientation of bonds and does not identify problems in translation. So, even if a complete α helix were misplaced by several angstroms, this would not necessarily be clear from the Q factor, except perhaps for a few residues with poor fits in the region linking the helix to the remainder of the structure.

If the orientation of internuclear bond vectors is truly random, the value of $\text{rms}(D^{\text{obs}})$ in Eq. (11) is given by¹²⁰:

$$\text{rms}(D^{\text{obs}}) = \{D_a^2[4 + 3R^2]/5\}^{1/2} \quad (12)$$

where D_a is the magnitude of the best-fitted alignment tensor and R its rhombicity [cf. Eq. (3e)]. In a given α helix or β sheet, N–H bond vectors tend to be roughly parallel to one another. Therefore, when amide N–H bond vectors are considered, their distribution in small proteins is frequently clustered and it may be preferable to calculate the denominator in Eq. (11) from Eq. (12). In cases where the error in the measurement exceeds the values of the dipolar coupling, Q can become greater than 1 when using Eq. (12), whereas it approaches 1 when simply using the root mean square of the measured couplings in the denominator of Eq. (11). Conversely, if the bond vectors have large random errors in the calculated structure relative to the true structure, the D_a obtained from Eq. (3) typically will be smaller than its true value, resulting in a smaller denominator when using Eq. (12) and consequently Q values that can be greater than 1.

Clore and Garrett proposed the same method as described above for evaluating the quality of protein structures, but refer to the quality factor as R .¹²¹ In their definition, R is simply $\sqrt{2}$ smaller than Q of Eq. (11), using the denominator

defined by Eq. (12). This R factor approaches 1 if the magnitude and rhombicity of the alignment tensor are known correctly, but the bond vector orientations in the structure under study are random relative to their true orientations.

8. Use of Dipolar Couplings in Structure Calculation

Although a dipolar coupling puts tight restrictions on the orientation of the corresponding internuclear vector, calculation of entire three-dimensional structures is not straightforward. A conceptually attractive metric method to build structures on the basis of dipolar couplings has been proposed by Brenneman and Cross,¹²² but this method requires some knowledge about what structural features are expected, and seems less suitable for proteins of fully unknown structure. One major problem is the twofold degeneracy in orientation, i.e., the inability to distinguish an isolated vector orientation from its inverse. In practice this means that if any of the backbone N–C^a or C^a–C' bonds is nearly parallel to any of the three principal axes of the alignment tensor, a 180° rotation of all atoms following this bond will yield the same dipolar couplings, and dipolar couplings therefore cannot establish unambiguously the orientation of the fragment preceding and following this bond.

A second, possibly even more serious problem is that dipolar couplings tend to compete with one another, when used in simulated annealing type programs. With NOE restraints, this is not the case. For example, if A and B are atoms of residue X, and C and D belong to residue Y, two experimental NOE restraints between atoms A and C and between B and D help one another, i.e., the A–C NOE already constrains the B–D distance. This results in a funnel-type energy landscape during the simulated annealing. With dipolar couplings, on the other hand, this is not the case. If, for example, an N–H bond is reoriented such that it satisfies the experimental D_{NH} dipolar coupling, this does not improve the agreement for the adjoining N–C' bond, unless the structure is already very close to the true structure. As a result, the energetic surface that includes the dipolar potential energy function tends to have a very large number of sharp local minima and is not amenable to simulated annealing for finding the global structure that provides best agreement with the dipolar couplings. As a result, most initial applications of dipolar couplings have focused on refinement of NMR structures, where the initial global fold is determined using conventional NOE restraints.

8.1. Structure Refinement with Dipolar Couplings

A common method for incorporating dipolar couplings into simulated annealing type structure determination has been developed for the program X-PLOR¹²³ by Tjandra *et al.*²⁸ In brief, a tetra-atomic pseudomolecule OXYZ is defined to

¹²⁰ G. M. Clore, M. R. Starich, C. A. Bewley, M. L. Cai, and J. Kuszewski, *J. Am. Chem. Soc.* **121**, 6513 (1999).

¹²¹ G. M. Clore and D. S. Garrett, *J. Am. Chem. Soc.* **121**, 9008 (1999).

¹²² M. T. Brenneman and T. A. Cross, *J. Chem. Phys.* **92**, 1483 (1990).

¹²³ A. T. Brunger, "X-PLOR: A System for X-Ray Crystallography and NMR," 3.1 Ed. Yale University Press, New Haven, CT, 1993.

represent the alignment tensor, where the OX, OY, and OZ bond vectors are orthogonal to one another. The O atom of this molecule is defined at a fixed position in space, away from the protein. An energetic penalty function term E_{dip} is defined that accounts for the difference between an observed dipolar coupling and the one predicted if the orientation of the alignment tensor were to correspond to that of OXYZ. As OXYZ freely reorients, it aligns itself to yield a best fit to the observed couplings during the simulated annealing process.

For a dipolar coupling between a pair of atoms P and Q, E_{dip} is given by

$$E_{\text{dip}} = k(D_{\text{PQ}}^{\text{calc}} - D_{\text{PQ}}^{\text{obs}})^2 \quad (13)$$

If E_{dip} is included in the regular simulated annealing protocol, the force constant k is increased exponentially during the cooling stage, typically starting at 10^{-4} kcal/Hz² for N–H dipolar couplings and increased to 0.5 or 1 kcal/Hz² at the final temperature. Force constants for other dipolar couplings are scaled according to the inverse square of their corresponding $D_{\text{max}}^{\text{AB}}$ [Eq. (1b)]. If the relative experimental uncertainty for some of the intrinsically smaller ¹⁵N–¹³C or ¹³C–¹³C couplings is significant, smaller scale factors may be used, such that after refinement the fit to the experimental couplings does not become tighter than the measurement error. Instead of scaling the force constant, all measured dipolar couplings can be scaled such that they correspond to a $D_{\text{max}}^{\text{AB}} = D_{\text{max}}^{\text{NH}}$, in which case a single force constant k may be used. However, for some of the scaled dipolar couplings with larger errors, smaller k values need to be used. In general, use of too high a k value results in poor convergence.¹²¹ Extensive cross validation may be used to determine optimal k values. For example, multiple sets of structures may be calculated for different k_{NC} values, and the set of structures that provides best agreement between predicted and experimentally observed D_{NH} couplings (not used as restraints) corresponds to the optimal value of k_{NC} .¹²⁴ As mentioned above, in no case should a force constant be chosen so high that the fit between experimental couplings and the structure (calculated with these dipolar coupling restraints included) becomes tighter than the experimental uncertainty in the measured couplings.

For methylenes, frequently only the sum of D_{CH1} and D_{CH2} can be measured.^{61,143} In this case, E_{dip} is simply given by

$$E_{\text{dip}} = k[(D_{\text{CH1}}^{\text{calc}} + D_{\text{CH2}}^{\text{calc}}) - (D_{\text{CH1}}^{\text{obs}} + D_{\text{CH2}}^{\text{obs}})]^2 \quad (14)$$

For tetrahedral methyl groups, rapid rotation scales the ¹³C–¹H dipolar coupling by $-1/3$. Thus, the threefold larger change in splitting observed for the outer ¹³C methyl quartet components is exactly opposite to that predicted for a proton located on the C–CH₃ bond vector, at the regular distance removed from the methyl carbon. As all constants related to bond length and gyromagnetic ratios are absorbed in the constants used in the X-PLOR routine, no separate pseudoatom needs to be defined

and the dipolar contribution to the outer quartet splitting, after multiplication by -1 , can be used directly to constrain the orientation of the C–CH₃ bond.⁶¹

For side chains, the effect of internal dynamics frequently can be particularly pronounced. In most cases, motion about an average position reduces the magnitude of the observed dipolar coupling relative to that expected for the time-averaged orientation, without changing its sign. Therefore, a conservative approach to including dipolar couplings measured for such side chains of unknown mobility simply uses the observed dipolar coupling as a lower bound. This is analogous to the NOE case, where frequently only upper limits for the NOE-derived distance restraints are used.

For ¹H–¹H interactions, the dipolar coupling is determined by the orientation of the interproton vector, but is also proportional to r_{HH}^{-3} . Except for methylene protons, where the interproton distance is essentially fixed at 1.8 Å, the energetic penalty term of Eq. (13) becomes also dependent on the distance. This presents no particular computational problem and the corresponding routines are available in X-PLOR.⁷⁶ As mentioned above, it can sometimes be difficult to unambiguously establish the sign of ¹H–¹H dipolar couplings. To address this problem, Eq. (13) can be modified to⁷⁶

$$E_{\text{dip}} = k(|D_{\text{PQ}}^{\text{calc}}| - |D_{\text{PQ}}^{\text{obs}}|)^2 \quad (15)$$

Unfortunately, this solution generally doubles the number of allowed orientations, and therefore aggravates the above-mentioned multiple minimum problem. Nevertheless, such absolute value dipolar couplings can be quite useful in structure calculation, in particular during the refinement process.

8.2. Identification of Protein Folds

If a best-fit superposition is made for two proteins with similar folds, corresponding bonds are expected to point in roughly parallel directions. Thus, a set of dipolar couplings measured for a given protein of unknown structure is expected to fit to a different protein that has a structure homologous to that of the unknown. The goodness of the fit depends primarily on the similarity of the two structures, but is also strongly dependent on the quality of the known structure. As mentioned above, the fit between dipolar couplings and a given structure can be expressed by the quality factor Q , which depends very strongly on the resolution at which an X-ray structure has been solved. For NMR structures determined in the absence of dipolar couplings, the Q factor frequently exceeds 50%, and it becomes difficult to identify such folds because of the “noise” in the bond vector orientations, even though the overall coordinate precision and accuracy may be reasonably close to the true structure.

Annala *et al.* were the first to exploit the dipolar coupling based homology search and showed that dipolar couplings measured for calerythrin indicated that this Ca²⁺-binding protein has a fold similar to sandworm sarcoplasmic

calcium-binding protein.¹²⁵ In related work, Meiler *et al.* identified ovomucoid as the protein that best fits the dipolar couplings of the N-terminal domain of rhodopsin, in agreement with their structural homology.¹²⁶ With the rapid expansion of the PDB database, it is expected that this dipolar homology search approach will become increasingly useful, as for an ever-increasing fraction of proteins homologous folds will be present in the PDB.

8.3. Angular Restraints from Dipolar Couplings

As discussed above, an energy surface that includes a term to account for the agreement between dipolar couplings and structure has an extremely large number of local minima, which makes it difficult to find the global minimum by simulated annealing methods. Meiler *et al.* propose to translate the dipolar couplings first into relative angular restraints, and to use these angular restraints in the simulated annealing protocol.¹²⁷ The principle of their method is easily understood by considering, for example, an axially symmetric alignment tensor, with $D_{\max}^{\text{NH}} = 5 \text{ Hz}$. If two amides both have dipolar couplings of 9 Hz, this means that each makes an angle of ca 15° with the z axis of the alignment tensor, i.e., an angle of less than 30° or larger than 150° , relative to one another. Similarly, if one coupling were found to be 9 Hz, and the second one -5 Hz (i.e., in the xy plane of the alignment tensor), the angle between the two vectors must be $90^\circ \pm 15^\circ$. However, if two couplings both are -5 Hz , no restraint can be derived as the corresponding vectors can reside anywhere in the xy plane. Although this latter example indicates that not all information contained in dipolar couplings is exploited in this approach, deriving direct angular restraints from dipolar couplings nevertheless has been demonstrated to be very useful in structure calculation. In this respect, it is important to note that intrinsically N dipolar couplings result in $N \times (N - 1)/2$ angular restraints. Even though the majority of these are "empty," in the sense that they do not exclude any angle between the corresponding vectors, and remaining restraints are not entirely independent from one another, the number of meaningful restraints remains rather large and is reported to be more amenable to simulated annealing than the dipolar couplings themselves.¹²⁷ Figure 15 provides an example of the energetic angular penalty function proposed by Meiler *et al.* and implemented by them in X-PLOR.

8.4. Molecular Fragment Replacement

As discussed above, dipolar couplings result in a highly rippled conformational energy surface that, in the absence of long-range distance information from

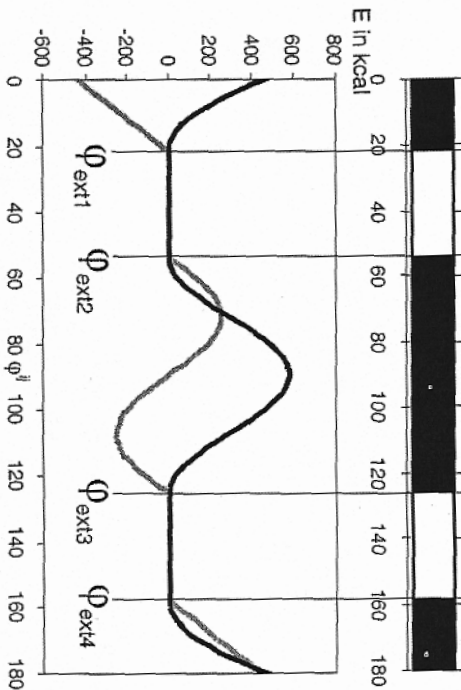


FIG. 15. Potential employed to confine the angle ϕ_{ij} between internuclear vectors i and j within the allowed range (white in upper bar) and exclude it from the forbidden range (black). A flat bottom potential is used for the allowed region, a parabolic potential for the margins close to 0 and π , and a $\cos^2 \Delta \phi_{ij}$ function for the inner forbidden part. The energy term is given by the black line and its derivative (negative force) by the gray line. Reprinted from Meiler *et al.*¹²⁷, with permission from Kluwer Academic Publishers.

NOEs, is unsuitable for conventional simulated annealing methods. However, it is important to realize that many of these local minima in the energy surface correspond to very unfavorable local conformations. If a starting model is used that is close to the true structure, convergence to the correct structure in a simulated annealing approach is generally much less of a problem. One simple method for obtaining such a starting model simply breaks the protein of interest in overlapping fragments of 7–10 residues in length. Then, the entire PDB or a representative subset is searched for fragments that provide the best fit to the experimental dipolar couplings.¹²⁸ In this respect, it is important to note that in a rigid protein, two separate fragments have the same values of A_a and A_r [cf. Eq. (3)]. Therefore, when searching the PDB for protein segments that would match the experimentally observed dipolar couplings, it is important that next to the goodness of the fit also the values of A_a and A_r are considered. If there is a high degree of consistency among the best hits, either the best fragment itself or the average backbone angles of the ensemble can be used for deriving a suitable starting model for the protein, which then can be refined either using a simple conjugate gradient procedure,¹²⁸ or by a low-temperature simulated annealing protocol¹²⁹ that

¹²⁵ A. Annala, H. Antio, E. Thulin, and T. Drakenberg, *J. Biomol. NMR* **14**, 223 (1999).

¹²⁶ J. Meiler, W. Petri, and C. Griesinger, *J. Biomol. NMR* **17**, 283 (2000).

¹²⁷ J. Meiler, N. Blomberg, M. Nilges, and C. Griesinger, *J. Biomol. NMR* **16**, 245 (2000).

¹²⁸ F. Delaglio, G. Kontaxis, and A. Bax, *J. Am. Chem. Soc.* **122**, 2142 (2000).

¹²⁹ J. J. Chou, S. Li, and A. Bax, *J. Biomol. NMR* **18**, 217 (2000).

includes a radius of gyration term to ensure appropriate compactness of the final structure.¹³⁰

8.5. Application to Nucleic Acids

Accurate structure determination of nucleic acids from NMR data is a notoriously difficult problem. The vast majority of NOEs is invariably intranucleotide or sequential, and very few long-range restraints are typically available. Moreover, there are five variable backbone angles connecting sequential nucleotides, vs only two angles between amino acids. Considering the paucity of long-range NOEs, dipolar couplings are likely to play a pivotal role in future nucleic acid structural studies.¹³¹ Results by Varani and co-workers^{132,133} and by Lynch and Puglisi¹³⁴ confirm the potential of these restraints in nucleic acid structure determination.

In a recent study, Tjandra *et al.* examined the structure of the so-called Dickerson dodecamer, d(CGGAAATTCCGCG)₂. Through the use of several different ¹³C/¹⁵N-labeled samples, some of these with stereospecific deuteration at the C2' and C5' methylene positions, it was possible to measure a nearly complete set of one-bond ¹H-¹³C and ¹H-¹⁵N dipolar couplings.¹³⁵ Structure calculation using X-PLOR-based simulated annealing then resulted in structures that showed generally good agreement with crystal structures determined for this dodecamer, but lacked several of the irregular pockers and backbone kinks, attributed to packing and Mg²⁺ coordination in the crystalline state. A superposition of Dickerson's original crystal structure and the NMR structure determined with dipolar couplings is shown in Fig. 16. For the center six base pairs, the two structures agree to within 0.6 Å with one another.

Remarkably, NOEs were equally well satisfied in the structures calculated with and without dipolar restraints, but the length of the dodecamer is much closer to that observed in the crystalline state when dipolar couplings are included. Other structural features, such as sequence dependence of basepair role, tilt, and helical twist, were found to be in good agreement with theoretical predictions, but only when dipolar couplings were included in the structure calculation. Sugar pucker amplitudes, on the other hand, were found to be too small, and presumably reflect dynamic averaging between a major 2'-endo conformational state and a minor 3'-endo conformer.¹³⁵

In the presence of the large number of dipolar couplings, extremely narrow bundles of structures (rmsd < 0.1 Å) were obtained, even when starting from fully

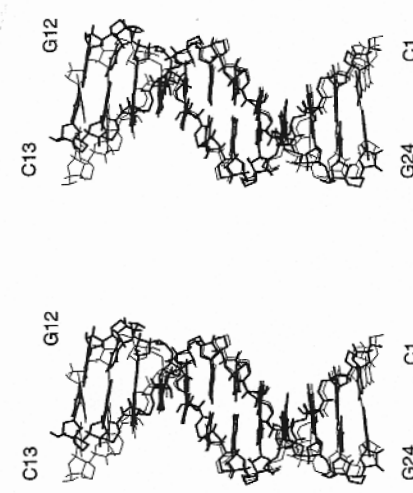


FIG. 16. Best-fit superposition of the crystal structure of d(CGGAAATTCCGCG)₂ (PDB entry 1BNA) and the NMR structure, determined primarily on the basis of dipolar couplings (1DUF) shown as thick and thin wireframe representation, respectively. From N. Tjandra, S. Tate, A. Ono, M. Kainoshio, and A. Bax, *J. Am. Chem. Soc.* **122**, 6190 (2000).

disordered structures. Clearly, such a high precision does not reflect the accuracy of the structure. The uncertainty in the magnitude of the alignment tensor used during the structure calculation was shown to affect the structure considerably, with changes in D_a of only 3% resulting in changes in the structure by as much as 0.3 Å. In practice, it will frequently be impossible to establish the magnitude of the alignment tensor to that level of accuracy, and therefore it is not likely that a true accuracy better than 0.3 Å is achievable from dipolar, NOE, and J coupling data. In principle, the magnitude of the alignment tensor can be a floating variable during structure calculation,¹³⁶ but this merely shifts the problem and does not necessarily increase the accuracy of the resulting structures over a systematic grid type variation in the alignment tensor.

Even in the presence of dipolar couplings, details related to the parameters and potentials used in structure calculation are likely to play a significant role in the final outcome of the structure calculations. This is evidenced, for example, by a

¹³⁶ F. Cordier, A. J. Dingley, and S. Grzesiek, *J. Biomol. NMR* **13**, 175 (1999).

¹³⁷ M. Ottiger and A. Bax, *J. Am. Chem. Soc.* **120**, 12334 (1998).

¹³⁸ G. Cornilescu and A. Bax, *J. Am. Chem. Soc.* **122**, 2168 (2000).

¹³⁹ M. Piotto, V. Sandek, and V. Sklenář, *J. Biomol. NMR* **2**, 661 (1992).

¹⁴⁰ Y. X. Wang, J. L. Marguñat, P. Wingfield, S. J. Stahl, S. Lee-Huang, D. Torchia, and A. Bax, *J. Am. Chem. Soc.* **120**, 7385 (1998).

¹⁴¹ L. E. Kay, P. Keifer, and T. Saarinen, *J. Am. Chem. Soc.* **114**, 10663 (1992).

¹⁴² S. Vijay-Kumar, C. E. Pugg, and W. J. Cook, *J. Mol. Biol.* **194**, 531 (1987).

¹⁴³ J. J. Chou and A. Bax, *J. Am. Chem. Soc.* in press, 2001.

¹⁴⁴ F. Delaglio, Z. Wu, and A. Bax, *J. Magn. Reson.* in press, 2001.

¹⁴⁵ N. Tjandra, S. Tate, A. Ono, M. Kainoshio, and A. Bax, *J. Biomol. NMR* **12**, 345 (1998).

- ¹ A. Bax, *Curr Opin Struct Biol.* **4**, 738 (1994).
² K. H. Gardner and L. E. Kay, *Annu Rev Biophys Biomol Struct.* **27**, 357 (1998).
³ B. T. Farmer and R. A. Venetis, in "Biological Magnetic Resonance," (N. R. Krishna and L. J. Berrine, eds.), Vol. 16, p. 75, Kluwer Academic/Plenum Publishers, New York, 1998.
⁴ K. Peruszhin, R. Rieck, G. Widter, and K. Wuthrich, *J. Am. Chem. Soc.* **120**, 6394 (1997).
⁵ K. Peruszhin, R. Rieck, G. Widter, and K. Wuthrich, *Proc. Natl. Acad. Sci. USA* **94**, 12366 (1997).

lorscopy) promises to increase the size of proteins amenable to solution NMR experiments. This so-called TROSY (Transverse Relaxation Optimized Spec-
selected, resulting in increased sensitivity and resolution in important classes from spins where the two competing relaxation fields partially cancel is
ived from chemical shift anisotropy (CSA) relaxation mechanisms.^{4,5} The signal de-
permits that makes use of cross-correlated spin relaxation between dipolar
and chemical shift anisotropy (CSA) relaxation mechanisms.^{4,5} The elegant class of ex-
More recently, Wuthrich's group has developed a very elegant class of ex-
periments that makes use of cross-correlated spin relaxation between dipolar
and chemical shift anisotropy (CSA) relaxation mechanisms.^{4,5} The signal de-
permits that makes use of cross-correlated spin relaxation between dipolar
and chemical shift anisotropy (CSA) relaxation mechanisms.^{4,5} The signal de-
permits that makes use of cross-correlated spin relaxation between dipolar
and chemical shift anisotropy (CSA) relaxation mechanisms.^{4,5} The signal de-

Introduction

By LEWIS E. KAY

Complex of Mattose Bimidine Protein and β -Cyclodextrin Molecular Weight Proteins: A Study Involving a [9] Nuclear Magnetic Resonance Methods for High

of regular helical structure relative to one another.¹²⁻¹³ Heteronuclear dipolar couplings will provide tight restrictions for orienting regions available. Even in cases where such information cannot be retrieved, one bond-dipolar couplings may suffice if quantitative interpretation of heteronuclear measurements of ^1H - ^1H couplings indicate that a smaller number of heteronucleic however, preliminary results obtained from novel experiments for quantitative couplings as was used for this dodecamer, this is a somewhat disappointing result. Considering that it is frequently will be impossible to get as complete a set of dipolar when an increasing fraction of the dipolar couplings is taken out of the calculation. continuous shift in the structure toward the one calculated without dipolar couplings